Author Manuscript Published OnlineFirst on January 15, 2021; DOI: 10.1158/2159-8290.CD-20-1109
Author manuscripts have been peer reviewed and accepted for publication but have not yet been edited.

# A CRISPR/Cas9-engineered *ARID1A*-deficient human gastric cancer organoid model reveals essential and non-essential modes of oncogenic transformation

Yuan-Hung Lo[1], Kevin S. Kolahi[2], Yuhong Du[3], Chiung-Ying Chang[2], Andrey Krokhotin[4], Ajay Nair[5], Walter D. Sobba[1], Kasper Karlsson[1,6], Sunny J. Jones[5], Teri A. Longacre[2], Amanda T. Mah[1], Bahar Tercan[7], Alexandra Sockell[6], Hang Xu[6], Jose A. Seoane[6], Jin Chen[8,9], Ilya Shmulevich[7], Jonathan S. Weissman[8], Christina Curtis[6], Andrea Califano[5], Haian Fu[3], Gerald R. Crabtree[2,4,10], Calvin J. Kuo[1*]

Department of Medicine, Divisions of Hematology[1] and Oncology[6], Stanford University School of Medicine, Stanford, CA 94305, USA

[2]Department of Pathology, Stanford University School of Medicine, Stanford, CA 94305, USA

[3]Department of Pharmacology and Chemical Biology and Emory Chemical Biology Discovery Center, Emory University School of Medicine, Atlanta, GA 30322, USA

[4]Howard Hughes Medical Institute, Stanford University School of Medicine, Stanford, CA 94305, USA

[5]Department of Systems Biology, Columbia University, New York, NY 10032, USA

[7]Institute for Systems Biology, Seattle, WA 98109, USA

[8]Howard Hughes Medical Institute, Department of Cellular and Molecular Pharmacology, University of California, San Francisco, CA 94158, USA

[9]Department of Pharmacology and Cecil H. and Ida Green Center for Reproductive Biology Sciences, UT Southwestern Medical Center, Dallas, TX 75390, USA

[10]Department of Developmental Biology, Stanford University School of Medicine, Stanford, CA 94305, USA

*Corresponding author: Calvin J. Kuo
Email: cjkuo@stanford.edu
Phone: 650-498-9047
Address: Stanford University School of Medicine, Lokey G2034A, 265 Campus Dr., Stanford, CA 94305, USA

**Running title**
Modeling *ARID1A*-deficient tumorigenesis in human organoids

**Key words**
ARID1A, Organoids, CRISPR/Cas9, FOXM1, BIRC5/survivin, WNT, Gastric Cancer

**Conflict of Interest Statement**
The authors declare no potential conflicts of interest

Author Manuscript Published OnlineFirst on January 15, 2021; DOI: 10.1158/2159-8290.CD-20-1109
Author manuscripts have been peer reviewed and accepted for publication but have not yet been edited.

**Abstract**

Mutations in *ARID1A* rank amongst the most common molecular aberrations in human cancer. However, oncogenic consequences of *ARID1A* mutation in human cells remain poorly defined due to lack of forward genetic models. Here, CRISPR/Cas9-mediated *ARID1A* knockout in primary *TP53*$^{-/-}$ human gastric organoids induced morphologic dysplasia, tumorigenicity and mucinous differentiation. Genetic Wnt/β-catenin activation rescued mucinous differentiation, but not hyperproliferation, suggesting alternative pathways of *ARID1A* KO-mediated transformation. *ARID1A* mutation induced transcriptional regulatory modules characteristic of MSI and EBV subtype human gastric cancer, including *FOXM1*-associated mitotic genes and *BIRC5/survivin*. Convergently, high-throughput compound screening indicated selective vulnerability of *ARID1A*-deficient organoids to inhibition of BIRC5/survivin, functionally implicating this pathway as an essential mediator of *ARID1A* KO-dependent early-stage gastric tumorigenesis. Overall, we define distinct pathways downstream of oncogenic *ARID1A* mutation, with non-essential Wnt-inhibited mucinous differentiation in parallel with essential transcriptional *FOXM1/BIRC5*-stimulated proliferation, illustrating the general utility of organoid-based forward genetic cancer analysis in human cells.

Author Manuscript Published OnlineFirst on January 15, 2021; DOI: 10.1158/2159-8290.CD-20-1109
Author manuscripts have been peer reviewed and accepted for publication but have not yet been edited.

**Statement of significance**

We establish the first human forward genetic modeling of a commonly mutated tumor suppressor gene, *ARID1A*. Our study integrates diverse modalities including CRISPR/Cas9 genome editing, organoid culture, systems biology and small molecule screening to derive novel insights into early transformation mechanisms of *ARID1A*-deficient gastric cancers.

Author Manuscript Published OnlineFirst on January 15, 2021; DOI: 10.1158/2159-8290.CD-20-1109
Author manuscripts have been peer reviewed and accepted for publication but have not yet been edited.

## Introduction

Alterations in the epigenetic landscape are a hallmark of cancer(1). The epigenetic state defines the permissible transcriptome as chromatin topology determines responses to oncogenes and tumor suppressors. Thus, chromatin regulators play critical roles in tumorigenesis, and their mutation is now appreciated as a pervasive feature of malignancy. The mammalian SWI/SNF (mSWI/SNF, BAF) chromatin remodeling complex actively remodels chromatin in an ATP-dependent fashion and renders DNA accessible to transcription factors and other DNA binding proteins(2) to govern development, homeostasis and disease(3–5).

*ARID1A*, also designated *BAF250a*, encodes a multifunctional BAF complex subunit that targets BAF to AT-rich enhancer DNA sequences, regulates transcription and recruits topoisomerase II to chromatin(6,7). *ARID1A* mutations rank amongst the most common molecular aberrations in human cancer(8–11) and are frequent in multiple cancer types such as ovarian clear-cell carcinoma (~57%), endometrioid carcinoma (~30%), urothelial carcinoma (~26%), cholangiocarcinoma (~19%), pancreatic ductal adenocarcinoma (~8%), and colorectal carcinomas (~8%)(12). Mutations in *ARID1A* occur in ~31% of all gastric adenocarcinomas, particularly in microsatellite instability (MSI) and Epstein-Barr virus-associated (EBV) subtypes, but also in the chromosomal instability (CIN) subtype with lower frequency(13–15). *ARID1A* mutations dysregulate BAF complex-mediated chromatin remodeling since this subunit directly interfaces with DNA and recruits other transcriptional co-activators(16). *ARID1A*'s function as a global chromatin conformation regulator underlies the pleiotropic effects observed when this gene is disrupted, and renders the study of ARID1A's role in oncogenesis especially challenging. Transgenic *Arid1a* knockout mouse models in embryo(17), ovarian(18), colon(19), small intestine(20), endometrium(21), pancreas(22–25), liver(26), and hematopoietic cells(27) have provided tremendous insight into *ARID1A*-associated tumorigenesis. However, despite these extensive mouse studies, forward genetic human models are crucially needed to elaborate

Author Manuscript Published OnlineFirst on January 15, 2021; DOI: 10.1158/2159-8290.CD-20-1109
Author manuscripts have been peer reviewed and accepted for publication but have not yet been edited.

mechanisms of *ARID1A*-dependent oncogenic transformation in a more clinically relevant context.

Organoid culture is a robust *in vitro* culture method that recapitulates many essential attributes of primary human tissue including 3-dimensional (3D) structure, multilineage differentiation, signaling nodes, histology, and pathology with high fidelity and thus represents an emerging approach to cancer biology(28). Bridging cell and tissue scales, organoids offer an attractive hybrid between transgenic mouse models and transformed 2D human cancer cell lines that enables an engineered “bottom up” approach to study temporal and sequential oncogenic events and permits the functional validation of oncogenic loci. Successful multi-hit oncogenic transformation of normal wild-type organoids to adenocarcinoma has been achieved by introducing simultaneous oncogenic mutations into tissues such as colon, stomach and pancreas(29–32).

Here, we utilize wild-type human gastric organoids to establish the first forward genetic human *ARID1A*-deficient oncogenic transformation model, using CRISPR/Cas9-engineered *ARID1A* depletion alongside mutation of *TP53,* a co-occurring tumor suppressor. These engineered *ARID1A*-deficient organoids mirror several clinicopathologic features of *ARID1A*-mutant gastric cancer. Coupled with a regulatory network-based analysis and high-throughput drug screening, we have leveraged this human organoid model to discover potential mechanisms underlying the role of *ARID1A* during oncogenic transformation of gastric epithelium.

Author Manuscript Published OnlineFirst on January 15, 2021; DOI: 10.1158/2159-8290.CD-20-1109
Author manuscripts have been peer reviewed and accepted for publication but have not yet been edited.

## Results

### *Establishment of clonal TP53 and TP53/ARID1A knockout human gastric organoid lines*

*Arid1a* is indispensable for stem-cell maintenance and self-renewal, as genetic deletion results in lethal compromise of gastrulation at E6.5, and knockout embryonic stem cells cannot be established(17,20,27,33). Consistent with these observations, using wild-type human gastric corpus organoids(34) from partial gastrectomy obesity surgeries, we could not expand and maintain *ARID1A* CRISPR/Cas9 KO derivatives in long-term culture. Four independent experiments were attempted, and a total of 12 clonal *ARID1A* CRISPR/Cas9 KO organoid lines were continuously tracked for at least two weeks. However, all of these *ARID1A* KO organoid lines eventually failed to grow, leading us to surmise that additional bypass mutation(s) could be needed. Thus, to establish an *ARID1A*-deficient human gastric cancer transformation model, we first disrupted *TP53*, the most frequently mutated locus (~49%) in gastric adenocarcinoma(14), by CRISPR/Cas9 into the same wild-type human gastric corpus organoids, followed by secondary CRISPR/Cas9 KO of *ARID1A*. Transient transfection of an all-in-one construct expressing both Cas9 and sgRNA targeting *TP53* exon 4 followed by a recently developed nutlin-3 functional selection(30,31) yielded numerous organoid colonies, whereas no growth was seen in non-transfected cells. After clonal expansion, a nutilin-3-resistant organoid clone harboring a 1 bp cytosine deletion (327delC; TTC<u>C</u>G to TTCG) within *TP53* exon 4 was chosen for further analysis **(Fig. 1A)**.

Serial genome editing in primary human organoids to generate sequential oncogenic mutations has been largely restricted by limited absolute knockout efficiency and a paucity of available functional selection strategies(35). To overcome these limitations and introduce inactivating mutations in *ARID1A* in these newly generated *TP53* KO gastric organoids, we utilized a two-vector, sequential lentiviral-based CRISPR/Cas9 system. First, *TP53* KO organoids were transfected with a Cas9 construct conferring blasticidin resistance and constitutive Cas9 protein expression was verified **(Fig. 1B)**. Cas9-expressing organoids did not

exhibit growth defects, suggesting low Cas9 toxicity after blasticidin selection. To quantify the efficiency of CRISPR/Cas9 cleavage, we delivered a second lentivirus containing a sgRNA targeting the GFP reporter in the same construct and a puromycin resistance gene **(Fig. 1C)**. In the parental *TP53* KO organoids, nearly all cells showed GFP expression after puromycin selection. However, in Cas9-expressing *TP53* KO organoids, over 95% of cells were GFP-negative as quantified by flow cytometry, indicating highly efficient CRISPR cleavage **(Fig. 1C)**.

We next applied this dual lentiviral system to *ARID1A* genetic knockout in *TP53*-null organoids. Of note, CRISPR can be mutagenic by introducing random insertions or deletions (indels) during cleavage, resulting in heterogenous cell populations. To address this potential pitfall and more precisely characterize sequelae of *ARID1A* loss in gastric tumorigenesis, we established a spectrum of clonal *TP53/ARID1A* DKO organoid lines by sgRNA targeting of *ARID1A* exon 1 or exon 11 in a lentiviral vector with BFP reporter. After lentivirus sgRNA-BFP delivery of Cas9-*TP53* KO organoids, single dissociated BFP positive cells were sorted into single wells of a 96-well plate, clonally expanded and *ARID1A* indels at sgRNA-targeted regions were confirmed by Sanger sequencing **(Fig. 1D)**. The corresponding wild-type organoids possessed wild-type *TP53* **(Fig. 1A)** and *ARID1A* **(Fig. 1D)** alleles. The loss of ARID1A expression, but not ARID1B, was further confirmed by Western blotting **(Fig. 1E)** and immunohistochemical (IHC) staining **(Fig. 1F)**. A total of five *TP53/ARID1A* DKO organoids lines were chosen for this study. In parallel, an empty lentiviral sgRNA-BFP vector was transduced into the same Cas9-*TP53* KO organoids, and represented the control. The *TP53* KO organoids (control) and *TP53/ARID1A* DKO organoids (*ARID1A* KO) were established, grown, maintained and passaged using identical culture conditions throughout this study. We performed whole-genome sequencing of control *TP53* KO, *TP53/ARID1A* DKO clone 3 (indels in *ARID1A* exon 1), and *TP53/ARID1A* DKO clone 5 (indels in *ARID1A* exon 11) at 3 months after *ARID1A* sgRNA delivery to outline the genetic background of these engineered organoids. The genome of the parental wild-type organoids was used as the reference. As expected, *TP53* mutation induced a moderate degree of chromosomal instability in both *TP53* KO and

Author Manuscript Published OnlineFirst on January 15, 2021; DOI: 10.1158/2159-8290.CD-20-1109
Author manuscripts have been peer reviewed and accepted for publication but have not yet been edited.

*TP53/ARID1A* DKO organoids **(Supplementary Fig. 1A)**, and a few shared and clonal-specific nonsynonymous mutations were detected **(Supplementary Fig. 1B).** Importantly, no additional canonical TCGA gastric cancer driver mutations were identified in either *TP53* KO or *TP53/ARID1A* DKO organoids, thus excluding promiscuous alteration of additional oncogenes or tumor suppressors **(Supplementary Fig. 1B)**.

***Loss of ARID1A promotes gastric malignancy***

To elucidate consequences of *ARID1A* loss in gastric tumorigenesis, we initially examined histology of *TP53* KO and *TP53/ARID1A* DKO organoids by hematoxylin and eosin (H&E) staining. *TP53* KO organoids harboring control sgRNA predominantly grew as variably-sized acini composed of a single layer of polarized epithelium **(Fig. 2A)**. Cytologically, the cells in *TP53* KO organoids were well-organized with an apically oriented cytoplasm and basally placed nucleus, indicating preservation of apicobasal polarity. In contrast, all five *TP53/ARID1A* DKO organoid lines exhibited different degrees of architectural complexity and cytologic changes characteristic of high-grade dysplasia, including but not limited to cribriform growth, stratification, increased nuclear to cytoplasmic ratios, and nuclear pleomorphism with nuclear membrane irregularities **(Fig. 2A)**. These features were rarely identified in the control *TP53* KO organoids. The cribriform features of *ARID1A* KO organoids resulted in multi-cystic organoids containing several lumina **(Fig. 2A)**, and epithelia were haphazardly arranged with loss of the distinctive apicobasal orientation evident on H&E stained histologic sections in *TP53* KO organoids. The latter observations, along epithelial stratification, raise the possibility that cell intrinsic apicobasal polarity is disrupted in *ARID1A*-deficient organoids **(Fig. 2A)**. Immunofluorescence staining of the apical-specific marker ZO1 further confirmed inappropriate basolateral ZO1 expression facing the extracellular matrix in a subset of *TP53*/*ARID1A* DKO organoid cells, suggesting disrupted apicobasal polarity **(Fig. 2B)**. Additionally, *TP53*/*ARID1A* DKO organoids exhibited several high-grade dysplasia cytologic features, including nuclear pleomorphism, nuclear membrane irregularities and conspicuous nucleoli **(Supplementary Fig. 2)**(36,37). Functionally,

Author Manuscript Published OnlineFirst on January 15, 2021; DOI: 10.1158/2159-8290.CD-20-1109
Author manuscripts have been peer reviewed and accepted for publication but have not yet been edited.

*TP53/ARID1A* DKO organoid lines proliferated more rapidly than *TP53* KO organoids, resulting in the larger size **(Fig. 2C)**, as well as increased EdU-positive cells **(Fig. 2D)**, revealing a growth advantage conferred by *ARID1A* loss. Consistent with these results, compared to *TP53* KO organoids, *TP53*/*ARID1A* DKO organoids exhibited higher metabolic activity **(Fig. 2E)**. Subcutaneous xenografts of *TP53* KO organoids showed poor *in vivo* engraftment and diminutive outgrowth (n=16, 18.75% success rate); however, *TP53*/*ARID1A* DKO organoids engrafted at a significantly greater rate (n=17, 76.47% success rate) and formed larger masses **(Fig. 2F)**. Of note, *TP53*/*ARID1A* DKO xenografts *in vivo* also reflected high-grade dysplasia **(Fig. 2F)**. Taken together, these results suggested that *ARID1A* mutation morphologically and functionally enhances tumorigenesis in primary human gastric organoids. Additionally, our review of histopathology and immunohistochemical ARID1A expression in a gastric cancer tissue microarray of 197 patients from Stanford Hospital indicated a significant inverse association between ARID1A staining and tumor grade **(Fig. 2G)**.

***Loss of ARID1A induces mucinous metaplasia***

Precancerous transformation of gastric epithelial cells is incited by alterations in genes involved in lineage differentiation and stem cell activity(38). Human gastric homeostasis is maintained, in part, by a gradient of canonical Wnt/β-catenin activity generated from the gland base, where the chief cells reside, extending to mucin-producing populations such as neck (TFF2+, LYZ+) and upper gland pit cells (TFF1+, MUC5AC+)(39,40). To determine if *ARID1A* loss altered organoid differentiation, we assessed several lineage-specific markers **(Fig. 3A)**. In comparison to *TP53* KO organoids, *TP53/ARID1A* DKO organoids upregulated TFF1, TFF2 and LYZ but the enteroendocrine marker CHGA was unaltered **(Fig. 3B)**. We further confirmed significantly up-regulation of additional pit cell markers, *GKN1* and *GKN2,* in *TP53/ARID1A* DKO organoids **(Supplementary Fig. 3A)**.

Next, we performed TFF1, MUC5AC, TFF2 and LYZ immunofluorescence staining of engineered organoids and the original cognate donor primary gastric tissues. In primary healthy

Author Manuscript Published OnlineFirst on January 15, 2021; DOI: 10.1158/2159-8290.CD-20-1109
Author manuscripts have been peer reviewed and accepted for publication but have not yet been edited.

tissues, TFF1 and MUC5AC were specifically expressed in the pit domain at gland tops **(Fig. 3C)**. In addition, TFF2 specifically marked mucous neck cells **(Supplementary Fig. 3B)** and LYZ labeled pit cells, with additional scattered positivity in gland bases **(Supplementary Fig. 3C)**. *TP53* KO organoids expressed very low levels of TFF1 and only sporadically expressed MUC5AC, TFF2 and LYZ. In contrast, *TP53/ARID1A* DKO organoids profoundly induced TFF1, MUC5AC, TFF2, and LYZ, consistent with acquisition of a mucinous phenotype **(Fig. 3C and Supplementary Fig. 3B-C)**. Chief cell mRNAs *LGR5*, *MIST1, PGC*, and *CPB1* were down-regulated in *TP53/ARID1A* DKO organoids **(Supplementary Fig. 3D)**.

Gastrointestinal cell fate decisions can increase mucin production in reaction to injury, a phenomenon termed mucous cell metaplasia(41,42). During metaplasia the epithelium is repopulated by cell lineages non-endemic to gastric tissues. Importantly, metaplastic transformation occurs in the earliest stages of progression of precancerous lesions to gastric cancer. We tested if *ARID1A* loss induced mucous cell metaplasia by Alcian blue staining, which marks acidic mucins in mucinous cancers but not normal stomach, and further does not stain pH-neutral mucins in healthy gastric epithelium **(Fig. 3D)**. Accordingly, Alcian blue-positive cells were significantly increased in all five *TP53/ARID1A* DKO lines, versus *TP53* KO organoids **(Fig. 3D)**. In addition, *in vivo* xenografts from *TP53/ARID1A* DKO organoids retained the mucinous phenotype with Periodic Acid-Schiff (PAS)-positive gastric pit cell-like and Alcian blue-positive intestinal goblet cell-like dysplastic cells **(Fig. 3E)**.

Interestingly, some Alcian blue and PAS double-positive mucin lakes were rimmed by Alcian blue-negative pit-like cells, suggesting an intermediate differentiation state between gastric-type and intestinal-type mucin-producing cells **(Supplementary Fig. 3E)**. *ARID1A* deficient mucinous organoid cells were indeed proliferative, as 21.3% of mitotic cells exhibited mucinous histology, which could be subdivided into goblet-like (1.3%) and pit-like (20%) cells **(Fig. 3F)**. Moreover, KI67-positive proliferating mucinous cells were identified **(Fig. 3G)**. To further investigate the gastric versus intestinal mucinous state in organoid xenografts, we performed IHC staining of CDX2, an intestinal epithelium specific transcription factor. Both *TP53*

Author Manuscript Published OnlineFirst on January 15, 2021; DOI: 10.1158/2159-8290.CD-20-1109
Author manuscripts have been peer reviewed and accepted for publication but have not yet been edited.

KO and *TP53/ARID1A* DKO xenografts exhibited clusters of CDX2-positive cells, indicating foci of intestinal metaplasia (IM) *in vivo* **(Fig. 3H)**. Interestingly, intestinal goblet cell-like MUC2+ cells were exclusively identified in *TP53/ARID1A* DKO xenografts, but not in *TP53/ARID1A* DKO organoids **(Fig. 3I)**, suggesting potential host tumor microenvironmental regulation of the IM phenotype. Accordingly, the gastric epithelium-specific tight junction protein CLDN18, was dramatically decreased in *TP53/ARID1A* DKO xenografts *in vivo*, versus *TP53/ARID1A* DKO organoids *in vitro* **(Fig. 3J)**. Of note, a small proportion of CLDN18-positive *TP53/ARID1A* DKO xenografts (<10%) resembled spasmolytic polypeptide-expressing metaplasia (SPEM)(42), a metaplastic mucous cell lineage, by co-expressing the chief cell digestive enzyme PGC and mucous neck cell specific marker MUC6 **(Fig. 3J)**.

We further confirmed these findings in gastric cancer patients by demonstrating a significant inverse correlation between ARID1A expression and mucin production by simultaneous ARID1A and Alcian blue staining of a 197-patient gastric cancer tissue microarray **(Fig. 3K)**. Of note, in a few cases of heterogeneous ARID1A tumor expression, mucin was present in association with tumor areas having low, but not high ARID1A expression **(Fig. 3K)**, again reiterating the mucous cell metaplasia associated with ARID1A loss.

***Loss of ARID1A inhibits canonical Wnt/β-catenin activity***

Wnt activity is inversely correlated with gastric mucinous differentiation since canonical Wnt signaling is lowest in the mucinous pit cell-containing regions occupying the apical-most domains of gastric glands(43) and withdrawal of Wnt and R-spondin from human gastric organoids directs cell fate from gland-type to mucin-expressing pit lineages(34). We thus hypothesized that organoid *ARID1A* KO induced the mucin-producing pit-like cell phenotype by impairing Wnt/β-catenin signaling **(Fig. 3)**. This was directly tested by delivering a Wnt-activated TOPflash luciferase construct containing an mCherry reporter by lentiviral-based transduction into our engineered organoids. An equivalent number of mCherry-positive single cells were sorted from *TP53* KO and *TP53/ARID1A* DKO organoids followed by quantification of

luciferase activity. Consistent with this model, Wnt/β-catenin-induced reporter activity was significantly reduced in all five *ARID1A*-deficient lines **(Fig. 4A)** despite their increased proliferation **(Fig. 2C-D)**.

To determine if the mucinous metaplasia induced by *ARID1A* loss could be rescued by constitutively activated Wnt signaling, we transduced an N-terminal truncated gain-of-function β-catenin (*CTNNB1*ΔN90) lentivirus bearing neomycin resistance into *TP53* KO and *TP53/ARID1A* DKO organoids, yielding *CTNNB1*ΔN90/*TP53* KO and *CTNNB1*ΔN90/*TP53/ARID1A* DKO organoid lines. The gain-of-function β-catenin mutant strongly induced TOPflash reporter activity **(Supplementary Fig. 4A)** and extinguished the ectopic MUC5AC, TFF1 and TFF2 expression in *TP53/ARID1A* DKO organoids, while LYZ was relatively unaffected **(Fig. 4B)**. Similarly, induction of MUC1, an apically-restricted, gastric cancer-associated transmembrane mucin(44), in *TP53/ARID1A* DKO organoids was profoundly reversed by *CTNNB1*ΔN90, reverting these organoids to a non-mucinous phenotype with re-establishment of apicobasal polarity indicated by uniformly apical MUC1 expression **(Fig. 4C)**. To delineate the inhibitory effect of extracellular Wnt and R-Spondin on the mucin-producing phenotype, organoids were grown for 9 days in the fully supplemented culture medium (WENR) followed by withdrawal of Wnt and R-Spondin from the medium (EN) for an additional 5 days to induce mucous cell differentiation. The expression of TFF1 and TFF2, but not LYZ and CHGA were increased in both *TP53* KO and *TP53/ARID1A* DKO organoids in the absence of Wnt and R-Spondin, suggesting withdrawal of Wnt stimulation is sufficient to induce mucinous differentiation **(Supplementary Fig. 4B)**. Taken together, these results suggested that the mucin-producing phenotype of *TP53/ARID1A* DKO organoids results from inhibition of Wnt/β-catenin activity, indicating a redirection of gland- to pit-like cell fate determination.

To mechanistically investigate *ARID1A* mutation-repressed canonical Wnt/β-catenin signaling and mucous cell differentiation, we studied Wnt/β-catenin-regulated transcripts upon *CTNNB1*ΔN90 rescue of either *TP53* KO or *TP53/ARID1A* DKO organoids. **(Fig. 4D and**

**Supplementary Table 1)**. Gene Ontology (GO) analysis of up-regulated genes showed enrichment of biological processes that are associated with Wnt activation, such as tissue development, regulation of Wnt signaling and epithelial to mesenchymal transition (EMT) **(Fig. 4E)**. As expected, Wnt/β-catenin target genes such as *TCF1*, *LEF1*, *ASCL2*, *AXIN2*, *CTNNB1*, *LGR5*, *LGR6* and *RNF43* were induced along with *MEX3A*(45), and *PROX1*(46) which mark injury-inducible intestinal stem cells **(Fig. 4F)**. In contrast, down-regulated gene GO terms implicated digestive tract development **(Fig. 4E)**. Consistent with *CTNNB1*ΔN90 abrogation of the mucinous phenotype, markers of gastric pit cells (*TFF1*, *LYZ*), gastric mucous neck cells (*TFF2*, *LYZ, AGR2*), and intestinal goblet cells (*TFF3*, *AGR2*, *REG4*) were significantly decreased **(Fig. 4F)** alongside transcription factors *SPDEF*, *SOX21*, *THRB* and *SIX2* **(Fig. 4G)**. Notably, *SPDEF* is a master transcription factor regulating mucin-producing cell differentiation and maturation across many tissue types, such as gastric mucous neck cells(47) and intestinal goblet cells(48,49). On balance, these results suggested *ARID1A*- and Wnt-dependent control of mucous cell differentiation via *SPDEF* regulation.

In addition to the mucinous phenotype, *CTNNB1*ΔN90/*TP53/ARID1A* DKO organoids rescued many dysplastic features characteristic of *TP53/ARID1A* DKO organoids, with reduced epithelial stratification and architectural complexity **(Fig. 4H)**. We next examined if the hyperproliferation phenotype of *TP53/ARID1A* DKO organoids **(Fig. 2C)** could be reverted by activated Wnt signaling. However, *CTNNB1*ΔN90 notably did not rescue the elevated cell proliferation of any of the five clonal *TP53/ARID1A* DKO organoid lines **(Fig. 4I)**. These results thus dissociated the non-essential Wnt repression-dependent mucous metaplasia from alternative undefined yet essential mechanisms governing *ARID1A* loss-associated hyperproliferation.

***ARID1A loss-associated gene regulatory modules recapitulates TCGA gastric cancers***

To identify the critical Wnt-independent biological processes governing the hyperproliferation associated with *ARID1A* loss, we investigated *ARID1A*-associated transcripts by bulk RNA-

Author Manuscript Published OnlineFirst on January 15, 2021; DOI: 10.1158/2159-8290.CD-20-1109
Author manuscripts have been peer reviewed and accepted for publication but have not yet been edited.

sequencing (RNA-seq) in the control *TP53* KO and two of the *TP53/ARID1A* DKO organoid lines. Compared to *TP53* KO organoids, the *TP53/ARID1A* DKO biological replicates contained 1,087 differentially expressed genes that were consistently up-regulated (472 genes) or down-regulated (675 genes) **(Fig. 5A and Supplementary Table 2)**. GO enrichment analysis of up-regulated genes in *ARID1A*-deficient organoids indicated several key biological processes including regulation of mitotic cell cycle, cell division, chromatin segregation, and cytoskeletal organization **(Fig. 5B and Supplementary Fig. 5)**. On the other hand, the top GO terms of the down-regulated genes in *ARID1A*-deficient cells included cell morphogenesis, nervous system development, cell differentiation, cell adhesion, cell migration, and negative regulation of cellular response to growth factor stimulus **(Fig. 5B and Supplementary Fig. 5)**. These findings were in agreement with our conclusions that *ARID1A* loss altered cell proliferation and differentiation in *TP53/ARID1A* DKO organoids **(Figs. 2, 3)**. Of note, the abnormal mitotic and chromatin segregation signatures suggested that *ARID1A* loss might be implicated in chromosome instability, consistent with our prior studies(7).

To gain deeper insights into how *ARID1A* loss influences gene regulatory architecture, we performed master regulator (MR) analysis using the VIPER(50) algorithm to elucidate *ARID1A*-regulated gene hierarchies(51). Akin to highly multiplexed gene reporter assays, VIPER infers the activity of 2,782 regulator proteins based on expression of their positively regulated and repressed transcriptional targets. Transcriptional targets were identified by analyzing a set of 200 TCGA stomach adenocarcinoma (STAD) gene expression profiles(14) using the ARACNe(52) algorithm. VIPER analysis identified several MRs representing candidate effector proteins that were significantly associated with *ARID1A* loss in two independent *TP53/ARID1A* DKO organoid lines **(Fig. 5C and Supplementary Table 3)**. FOXM1, a classical proliferation-associated transcription factor that is intimately involved in tumorigenesis(53), was listed as the top-ranked MR that was differentially enriched in both *TP53/ARID1A* DKO organoid biological replicates versus the control *TP53* KO organoids. Consistent with this result, several *FOXM1* targets, such as *BIRC5, CKS1B, CDC25C, CCNB1, CCNB2, CDK1*, *AURKA* and

Author Manuscript Published OnlineFirst on January 15, 2021; DOI: 10.1158/2159-8290.CD-20-1109
Author manuscripts have been peer reviewed and accepted for publication but have not yet been edited.

*AURKB*, were simultaneously upregulated in parallel with *FOXM1* in *ARID1A*-deficient organoids **(Fig. 5C and Supplementary Table 4)**. The upregulation of the *FOXM1* targets BIRC5 and AURKB was further confirmed by Western blotting **(Fig. 5D)**. Notably, the global MR profile of *ARID1A*-deficient organoids revealed strong overlap with MRs independently identified in TCGA STAD gastric cancers, with particularly significant similarity to STAD MSI ($p<7.56E-12$) and EBV ($p<0.03$) clusters where *ARID1A* mutations are highly enriched(14,15) but not GS ($p>1$), CIN ($p>0.97$), and HM-SNV ($p>0.23$) subtypes **(Fig. 5E)**. In addition, compared to a gastric cancer patient-derived organoid (PDO) data set that was established in previous studies(54), the MR profile of *ARID1A*-deficient organoids again exhibited significant similarity to the MSI subtype PDOs **(Fig. 5F)**.

**ARID1A deletion confers therapeutic vulnerability to Survivin inhibition**

A potential advantage of the use of isogenic paired *TP53* KO and *TP53/ARID1A* DKO organoids engineered from non-neoplastic gastric tissue is a reduced likelihood of simultaneous confounding co-occurring mutations that are common to transformed cancer cell lines, as confirmed by lack of driver alterations upon whole genome sequencing **(Supplementary Fig. 1)**. Thus, the syngeneic and low background somatic mutational burden of these engineered organoids provided a unique opportunity to study *ARID1A* growth dependencies in a system having reduced interference from modifier loci. Thus, we tested *ARID1A*-specific growth dependencies by high-throughput small molecule screening of an FDA-approved and bioactive chemical library (2,036 compounds) in *TP53/ARID1A* DKO versus control *TP53* organoid lines **(Fig. 6A)**. *TP53/ARID1A* DKO organoids were dissociated into smaller clusters, re-plated into 384-well plates, cultured for 5 days followed by drug treatment and cell viability was quantified after 3 additional days **(Fig. 6A)**. Notably, this screening system exhibited robust assay performance, with signal-to-background (S/B) ratio > 8 and Z' > 0.5 **(Fig. 6B)**. To discover compounds exhibiting selective synthetic lethality with *ARID1A* deficiency, we performed 12-point concentration counter-screening in the control *TP53* KO versus two additional

Author Manuscript Published OnlineFirst on January 15, 2021; DOI: 10.1158/2159-8290.CD-20-1109
Author manuscripts have been peer reviewed and accepted for publication but have not yet been edited.

*TP53/ARID1A* DKO lines for the top 50 hits from the initial primary DKO organoid screening. Among these, several candidates such as YM-155, BMS-526924, HS-173 and Torin-2 selectively inhibited proliferation of *TP53/ARID1A* DKO versus *TP53* KO organoids, whereas many hits such as AP-26113 showed no obvious differences **(Supplementary Fig. 6A)**.

We then performed secondary counter-screening with repurchased compounds to repeat and further confirm enhanced sensitivity in *TP53/ARID1A* DKO organoids. While some variability in the magnitude of sensitivities were observed, the results of the secondary confirmatory assay were generally consistent with our primary screen, yielding 14 candidate compounds that selectively enhanced killing of *ARID1A*-mutant organoids **(Supplementary Fig. 6B)**. Consistent with previous studies of *ARID1A*-mutated cancer cells, engineered *ARID1A*-deficient gastric organoids were selectively sensitive to histone deacetylase (HDAC) inhibitors(55,56) and PI3K/AKT inhibitors(57,58) **(Supplementary Fig. 6B)**. Among these compounds, *ARID1A*-deficient gastric organoids were also sensitive to YM-155, a small molecule inhibitor of BIRC5/survivin(59), a member of the inhibitor of apoptosis (IAP) family, which inhibits caspase-mediated apoptosis(60) and controls mitotic spindle dynamics and chromosome segregation(61) **(Supplementary Fig. 6A-B).** We additionally confirmed the potent YM-155 repression of BIRC5 protein in *TP53* KO and *TP53/ARID1A* DKO organoids **(Supplementary Fig. 6C)**. Crucially, YM-155 exhibited selective lethality with *ARID1A* mutation consistently across all five *TP53/ARID1A* DKO lines (average $IC_{50}$=0.03 μM) versus the two *TP53* KO lines (average $IC_{50}$=0.23 μM) **(Fig. 6C-D)**.

We further evaluated the therapeutic effect of YM-155 in conventional 2D gastric cancer cell lines, as opposed to oncogene-engineered organoids. Six isogenic pairs of *ARID1A* wild-type and mutant cancer cell lines were generated by CRISPR/Cas9, and sensitivities to YM-155 were compared. In contrast to 3D engineered organoids, *ARID1A* KO 2D gastric cancer cell lines did not exhibit selective sensitivity to YM-155 **(Supplementary Fig. 7)**. These results indicated that highly transformed gastric cancer cell lines are less dependent on BIRC5/survivin

Author Manuscript Published OnlineFirst on January 15, 2021; DOI: 10.1158/2159-8290.CD-20-1109
Author manuscripts have been peer reviewed and accepted for publication but have not yet been edited.

after *ARID1A loss* than our DKO organoids, which appear to harbor only *TP53* and *ARID1A* oncogenic driver mutations and thus model early gastric cancer **(Supplementary Fig. 1A-B)**.

**Rescue and functional independence of *ARID1A* KO-regulated BIRC5/survivin and Wnt pathways**

To test if constitutive expression of BIRC5 was sufficient to rescue YM-155-associated *ARID1A* synthetic lethality, we lentivirally overexpressed MYC-DDK-tagged BIRC5 in *TP53* KO versus *TP53/ARID1A* DKO organoid lines **(Fig. 6E)**. As expected, single *TP53* KO control organoids exhibited YM-155 insensitivity at the $IC_{50}$ of 0.03 μM for *TP53/ARID1A* DKO organoids, which was not altered by BIRC5 overexpression. However, the YM-155 hypersensitivity of multiple independent *TP53/ARID1A* DKO organoid lines was significantly rescued by BIRC5 overexpression, which additionally confirmed the specificity of YM-155 for BIRC5 **(Fig. 6F)**. This unexpected convergence between the MR analysis, in which the mostly highly ranked hit was a *ARID1A* KO-induced FOXM1→BIRC5/survivin regulatory node with concurrent upregulation of *FOXM1* mRNA and *BIRC5* mRNA and protein **(Fig. 5)**, and the small molecule screen, revealing selective sensitivity of *ARID1A* KO organoids to the BIRC5/survivin inhibitor YM-155 **(Fig. 6)**, functionally implicated FOXM1→BIRC5/survivin as an essential pathway mediating hyperproliferation following *ARID1A* loss. Consistent with these findings in the organoids, *BIRC5* expression was significantly higher in TCGA STAD patients harboring *ARID1A* mutations **(Supplementary Table 5)**.

We then probed the functional independence of the *ARID1A* KO-induced, YM-155-senstive, FOXM1→BIRC5/survivin essential proliferation pathway, as distinct from the non-essential Wnt-regulated mucinous differentiation pathway. Importantly, YM-155 did not inhibit Wnt-dependent mucous metaplasia in *ARID1A*-deficient organoids **(Fig. 6G)**. LEF1 and TCF1 are two Wnt/β-catenin targets that are robustly induced by the *CTNNB1*ΔN90 gain-of-function β-catenin mutant **(Fig. 6H, lane 1 versus lane 3)**. As expected, LEF1 and TCF1 proteins were decreased in *TP53/ARID1A* DKO organoids having impaired Wnt signaling, versus control *TP53* organoid

Author Manuscript Published OnlineFirst on January 15, 2021; DOI: 10.1158/2159-8290.CD-20-1109
Author manuscripts have been peer reviewed and accepted for publication but have not yet been edited.

lines **(Fig. 6H, lane 1 versus lanes 4, 7 and 10)**. However, YM-155 did not revert the *ARID1A* KO-associated decrease in LEF1 or TCF1 protein **(Fig. 6H, lanes 1 versus 2, 4 versus 5, 7 versus 8, 10 versus 11)**, indicating that YM-155 did not affect Wnt/β-catenin activity. Consistent with these observations, Wnt/β-catenin-induced TOPflash reporter activity was also not altered by YM-155 treatment **(Fig. 6I)**. Conversely, *CTNNB1*ΔN90 Wnt pathway activation did not rescue the expression of BIRC5 **(Fig. 6J)**, or the selective YM-155 proliferation sensitivity of *ARID1A*-deficient organoids **(Fig. 6K)** despite potently reversing the mucinous metaplasia phenotype **(Fig. 4B-C)**. In total, these selective perturbation results confirmed the independent functionality of the *ARID1A* KO-induced Wnt/mucinous metaplasia versus FOXM1→BIRC5/survivin-mediated proliferation pathways.

Author Manuscript Published OnlineFirst on January 15, 2021; DOI: 10.1158/2159-8290.CD-20-1109
Author manuscripts have been peer reviewed and accepted for publication but have not yet been edited.

## Discussion

Primary human organoids have proven to be invaluable models of tumorigenesis(28). Organoids mimic oncogenic transformation on a collective tissue scale and accurately replicate the *in vivo* biology of their original native tissues. Coupled with contemporary experimental methods, organoid systems provide enormous experimental flexibility and capacity for studying molecular mechanisms of gene function in human cells. CRISPR/Cas9 gene editing of primary human organoids from various tissues including colon(30,31,62), stomach(32), pancreas(63,64) , breast(65) and liver(66) has contributed tremendous mechanistic insight into the functional basis of diverse oncogenic loci identified from large-scale next-generation sequencing studies of human cancers. Here, we leveraged primary human gastric organoids to establish the first forward genetic human *ARID1A* transformation model, whose multi-omic analysis revealed phenotypic and functional recapitulation of numerous features of *ARID1A*-mutated gastric cancer.

The inability to establish *ARID1A* KO organoids from wild-type human gastric organoids could originate in the anaphase bridge formation and G2/M cell cycle arrest upon loss of BAF subunits(7). *TP53* deficiency, as in the current study, may bypass this arrest, allowing establishment of organoids mutated in both *ARID1A* and *TP53*. Although concomitant mutation of *ARID1A* and *TP53* occurs sporadically (~4-13%) in human gastric cancers and ~30% of MSI gastric cancer(14,15,67), the engineered *TP53/ARID1A* DKO organoids nevertheless faithfully recapitulate numerous features of *ARID1A*-mutated gastric cancer; similar studies could be extended to model *ARID1A* loss in the context of other driver mutations.

Notably, *ARID1A* KO elicits global transcriptional regulatory programs significantly reminiscent of MSI- and EBV-type gastric cancers, precisely those subtypes in which *ARID1A* mutation is most prevalent(14,15). Moreover, the absence of engineered MSI mutations in *ARID1A*-defieicient organoids suggests that *ARID1A* loss may be a major determinant of the overall transcriptional regulatory program of MSI stomach adenocarcinoma. Crucially, our

Author Manuscript Published OnlineFirst on January 15, 2021; DOI: 10.1158/2159-8290.CD-20-1109
Author manuscripts have been peer reviewed and accepted for publication but have not yet been edited.

multiscale analysis of *ARID1A* KO organoids, integrating transcriptional, small molecule and computational approaches, defines a bifurcated model of *ARID1A*-dependent oncogenic transformation where non-essential Wnt-regulated mucinous metaplasia is distinct from essential YM-155-sensitive, FOXM1→BIRC5-regulated proliferation **(Fig. 7)**.

Mechanistically, *ARID1A* loss inhibits canonical Wnt/β-catenin activity leading to a redirection of gland- to pit-like cell fate determination. During homeostasis, gastric cell determination is maintained by a gradient of canonical Wnt/β-catenin activity that is established and most intense at the gland base, and extends up toward the mucin-producing pit cells in the upper gland where canonical Wnt/β-catenin activity is virtually absent(43). Emerging evidence suggests Wnt and R-Spondin agonists are critical microenvironmental cues for maintaining gastric stem cells(34,68,69). Consistent with this, *ARID1A*-deficient organoids displayed reduced canonical Wnt/β-catenin signaling, accompanied by a shift to pit-like mucin-producing lineage differentiation which was potently rescued by constitutive β-catenin activation. Of note, constitutive β-catenin activation significantly downregulated several gastric mucous cell and intestinal goblet cell genes, including *SPDEF*, encoding a transcription factor regulating epithelial goblet cell differentiation(47,48). Consistent with these results, previous studies identify SPDEF as a Wnt-responsive gene(48) that functions as a colorectal cancer tumor suppressor by regulating Wnt signaling(70,71). Together with the inverse relationship between ARID1A expression and mucinous differentiation in human gastric cancer microarrays, our findings confirm prior transgenic mouse studies where *Arid1a* loss promotes mucinous tumorigenesis in colon(19) and pancreas(22–24) but where a molecular mechanism was not established. In contrast, non-mucinous differentiation associated with *Arid1a* mutation occurs in ovarian and uterine tumors(18,21). Thus, lineage metaplasia may be a pervasive feature of *ARID1A*-deficient cancer, which our studies reveal can be driven by Wnt pathway dysregulation.

Surprisingly, despite robust Wnt-dependency of *ARID1A* loss-induced mucous metaplasia, this pathway did not regulate cell division, indicating non-essentiality. Instead, the unexpected convergence of our master regulator and small molecule selective lethal screens identified a

YM-155-sensitive FOXM1→BIRC5 transcriptional node as a essential regulator of *ARID1A* KO-induced proliferation. The functional independence of the Wnt/mucin versus FOXM1→BIRC5/proliferation pathways is attested by the inability of β-catenin rescue to alter YM-155 sensitivity, while conversely YM-155 does not reverse Wnt-dependent mucinous differentiation or target expression.

Several studies have pursued discovery of targets exhibiting synthetic lethality with *ARID1A* deficiency in transformed cancer cell lines. Such ARID1A selective lethal compounds include inhibitors of EZH2 methyltransferase, a PRC2 core subunit that opposes BAF complex activity(72,73) and glutathione synthesis antagonists(74). Our results clearly indicate that *ARID1A* mutation confers selective sensitivity to BIRC5/survivin inhibition in engineered gastric organoids, reflecting early-stage gastric tumorigenesis. In contrast, multiple conventional 2D cancer cell lines did not exhibit selective sensitivity to BIRC5/survivin inhibition. Thus, BIRC5 dependency appears more stringent during earlier stages of *ARID1A*-deficient gastric oncogenesis, as in engineered organoids, while late-stage gastric cancers may possess redundant pro-survival mechanisms. We also cannot exclude confounding effects on drug sensitivity from 2D cancer cell line versus 3D engineered organoid culture, which can influence oncogenic phenotypes(75), or from genetic drift and resistance mechanisms in long-passaged cell lines. Thus, further work will be required to explore YM-155 efficacy in established gastric cancer and define the range of *ARID1A*-deficient malignancies for which YM-155 may be effective.

Mouse models have proven invaluable for study of molecular mechanisms underlying gastric metaplasia and its neoplastic progression. However murine models, while recapitulating early-stage gastric mucous cell hyperplasia and SPEM, are limited in modeling the later stages of carcinogenesis in humans, such as progression to IM, high-grade dysplasia, and infiltrating adenocarcinoma. Our engineered *TP53/ARID1A* DKO human organoids recapitulate high-grade dysplasia *in vitro* and acquired intestinal goblet cell features *in vivo*, the latter suggesting that stromal and/or inflammatory cells within the tumor microenvironment may promote development

Author Manuscript Published OnlineFirst on January 15, 2021; DOI: 10.1158/2159-8290.CD-20-1109
Author manuscripts have been peer reviewed and accepted for publication but have not yet been edited.

of late-stage gastric tumors. Interestingly, upon *in vivo* implantation, ~10% of *TP53/ARID1A* DKO organoid cells exhibit SPEM features, indicating that *ARID1A* loss could potentially predispose to SPEM, possibly in concert with environmental cues. Thus, engineered human tumor organoids together with *in vivo* xenotransplantation provide a valuable platform for studying previously inaccessible stages of human gastric cancer development. Future studies will be required to determine whether additional oncogenic drivers or microenvironmental cues facilitate evolution of *ARID1A*-deficient cells to metastatic adenocarcinoma.

Overall, our forward genetic study of engineered *ARID1A*-deficient human gastric organoids enabled a functional deconstruction of essential versus non-essential mechanisms of early *ARID1A*-dependent tumorigenesis. These analyses were greatly facilitated by the synthesis of genome-scale omics approaches, high-throughput small molecule screening and computational models, affording mechanistic insights into the genesis of *ARID1A*-deficient gastric cancer. Conceivably, analogous multimodal approaches to oncogene-engineered organoids may be further generalizable to additional cancer-associated loci and malignancies, yielding clinically relevant insights regarding cancer initiation and ultimately therapy.

**Acknowledgements**

We thank generous support from NIH fellowship K00CA212433 (Y-H.L.), a Swedish Research Council International Postdoctoral Fellowship (K.K.), Stanford Bio-X Undergraduate Fellowship (W.D.S.), the NCI Cancer Target Discovery and Development (CTD2) Network (C.J.K., H.F., A.C. and C.N.C.), NIH U01CA217875 to H.F., NIH R01CA163915 to G.R.C and grants from the NIH (U01CA217851, U54CA224081, U01CA199241 and U19 AI116484), Emerson Collective and Ludwig Cancer Research to C.J.K.

**Author Contributions**

Y-H.L., K.S.K., W.D.S., K.K. and A.S. generated and analyzed organoids. Y.D. performed small molecule screening. C.-Y.C. performed RNA-seq, A.K., J.A.S. B.T., H.X., I.S. and C.C. analyzed genomic data. A.N., S.J.J., and A.C. performed master regulator analysis. T.A.L. provided gastric cancer tissue microarrays. J.C. and J.S.W. provided reagents for CRISPR/Cas9 genome-editing. Y.-H.L., K.S.K. and C.J.K. wrote the manuscript. Y.-H.L., H. F., G.R.C. and C.J.K. conceived and designed experiments.

Author Manuscript Published OnlineFirst on January 15, 2021; DOI: 10.1158/2159-8290.CD-20-1109
Author manuscripts have been peer reviewed and accepted for publication but have not yet been edited.

## Methods

***Cell lines and maintenance.*** L-WRN cells (ATCC, CRL-3276) that produced Wnt-3A/R-spondin/Noggin conditional media, and HEK293T cells were maintained in DMEM (Life Technologies, #11995-073) supplemented with 10% FBS. Gastric cancer cell lines were purchased from ATCC. SNU-16, AGS, NCI-N87 and MKN7 cells were maintained in RPMI1640 supplemented with 10% FBS. HGC27 cells were maintained in DMEM supplemented with 10% FBS. KATO-III cells were maintained in DMEM supplemented with 20% FBS. All cells were cultured at 37°C with 5% $CO_2$. All cell lines have been tested for mycoplasma at least once every 6 months.

***Organoid culture media.***

The organoid culture media contained Advanced DMEM/F-12 (Thermo Fisher Scientific, #12634028) with 0.5% Penicillin/Streptomycin/Glutamine (Thermo Fisher Scientific, #10378016), 5% FBS, 1 mM HEPES (Thermo Fisher Scientific, #15630080), 1 mM N-Acetylcysteine (Sigma, A9165), 1X B-27 Supplement (Thermo Fisher Scientific, #12587001), 500 nM A83-01 (Tocris Bioscience, #2939), 1X GlutaMax Supplement (Thermo Fisher Scientific, #35050061), 10 μM SB-202190 (Biogems, #1523072), 10 mM Nicotinamide (Sigma, #N0636), 50 ng/mL EGF (PeproTech, AF-100-15), 100 μg/mL Normocin (InvivoGen, ant-nr-1), 10 mM Gastrin (Sigma, G9145), 200 ng/mL fibroblast growth factor (FGF) (Peprotech, #100-26), and 50% Wnt-3A/R-spondin/Noggin conditioned media.

***Establishment of normal gastric organoid cultures.*** Clinical samples used for gastric organoid establishment were obtained from gastric corpus of patients at Stanford University Hospital's Tissue Procurement Shared Resource facility. Healthy gastric tissues were collected by surgical resection. Gastric organoids were established as previously reported(34). Briefly, surgical specimens were washed vigorously three times with sterile, cold phosphate-buffered

saline (PBS) in a 15 mL conical tube, and then were dissected into smaller pieces in cold chelation buffer (5.6 mM $Na_2HPO_4$, 8.0 mM $KH_2PO_4$, 96.2 mM NaCl, 1.6 mM KCl, 43.4 mM Sucrose, 54.9 mM D-Sorbitol, 0.5 mM DTT) plus 10 mM EDTA. The tissues were incubated 4ºC for 3-5 hours in a rocking chamber. After incubation, tissues were washed by fresh cold chelation buffer and vigorously shaken by hands. After shaking, the supernatant was checked for the presence of gastric crypts. This step was repeated 8-10 times and each wash produced supernatant containing gastric crypts that were examined under bright-field microscope. Finally, crypts collected from different fractions were combined and centrifuged at 600 g at 4°C for 5 minutes. Gastric crypts were resuspended in Matrigel (R&D systems, Basement Membrane Extract type 2) and plated in a 24-well plate. After Matrigel polymerization, organoid culture media was added to each well (described above) plus 10 μM Y-27632 (Peprotech, #1293823) and 3 μM CHIR-99021 (R&D Systems, #4223). After 3 days, the media was changed to organoid culture media without Y-27632 and CHIR-99021, and cultures were maintained in organoid culture media with routine media changes occurring every 3-4 days until subsequent passage. Fibroblast growth factor (FGF) was dispensable for engineered *TP53* KO and *TP53/ARID1A* DKO organoids. Organoids were passaged to prevent overgrowth every 10-14 days. For passaging, organoids were washed by PBS and mechanically dissociated into smaller pieces by pipetting and resuspension in TrypLE™ (Invitrogen, #12604-012) at 37°C for 10-20 minutes. After incubation, fetal bovine serum (FBS) was added to quench TrypLE™ activity. Organoids were then centrifuged at 600 g for 5 minutes and washed once using organoid culture media before resuspension in matirgel and plating onto a new 24-well plate.

***Guide RNA expression vector cloning*.** The lentiviral sgRNA vectors were generously provided by Dr. Jonathan Weissman(76,77). The sgRNA vector was digested by BstXI (New England BioLabs, R0113) and BlpI (New England BioLabs, R0585) at 37°C for 6 hours. The linearized vectors were separated on a 1% agarose gel. Linearized vectors were cut and then purified by QIAquick Gel Extraction Kit (Qiagen, #28706). The lentiviral sgRNA expression

vectors were cloned by inserting annealed sgRNA oligos into the linearized sgRNA vectors. The ligation of the linearized vectors and the annealed sgRNA oligos were completed by T4 DNA ligase (New England BioLabs, M0202) at 25°C for 2 hours. Ligation reactions were transformed into Stellar Competent *E. coli* Cells (TaKaRa, #636763) following the manufacturer's instructions. Competent cells were plated on LB agar plates supplemented with 100 µg/mL carbenicillin and incubated at 37°C overnight. Colonies were randomly picked from each plate and inoculated into 4 mL LB supplemented with 100 µg/mL carbenicillin and then grown at 37°C for 14 hours. The lentiviral sgRNA expression vectors were purified by QIAprep Spin Miniprep Kit (Qiagen, #27106) for subsequent confirmation by Sanger-sequencing. The sgRNA sequences used in this study were listed in the key resources table.

***Generation of clonal organoid lines.*** Organoids were washed by PBS dissociated with TrypLE™ (Invitrogen, #12604-012) for 30 minutes at 37°C. Cell clumps were removed using 35 mm cell strainer (BD Falcon, #352235) and the flow-through was pelleted at 600 g at 4°C for 5 minutes. Cells pellets were resuspended in organoid culture media with 10 µM Y-27632 (Peprotech, #1293823). Single cells were sorted in single wells of a 96-well plate. The 96-well plate was pre-coated by 10 µL Matrigel (R&D systems, Basement Membrane Extract type 2) and covered by 100 µL organoid culture media. FACS Aria II (BD Biosciences) equipped with a 100 mm nozzle was used for cell sorting. Wells containing a single organoid 12-14 days after cell sorting were dissociated with TrypLE™ and replated for clonal expansion. The clonal lines were verified by Sanger-sequencing, immunoblot analysis, or immunostaining. For Sanger-sequencing, genomic DNA was isolated from organoids by using DNeasy blood and tissue kit (Qiagen, #69506). The targeted loci were amplified by PCR using Phusion High-Fidelity DNA Polymerase (New England BioLabs, M0530) and then sequenced directly. Primers for PCR amplification and Sanger-sequencing used in this study were listed in the key resources table.

Author Manuscript Published OnlineFirst on January 15, 2021; DOI: 10.1158/2159-8290.CD-20-1109
Author manuscripts have been peer reviewed and accepted for publication but have not yet been edited.

***Generation of lentivirus.*** Lentiviral plasmids were co-transfected with viral packaging plasmid psPAX2 (Addgene, #12260) and viral envelope plasmid pCMV-VSV-G (Addgene, #8454) into 293T cells by Lipofectamine 2000 (Invitrogen, #11668-019) following the manufacturer's instructions. Lentiviral supernatants were collected at 48 hours and 72 hours post-transfection and concentrated by PEG-it Virus Precipitation Solution (System Biosciences, LV825A-1). Precipitated lentiviral particles were pelleted at 1500 g at 4°C for 30 minutes and resuspended in organoid culture media containing 10 μM Y-27632 (Peprotech, #1293823). Lentiviral plasmids used in this study were listed in the key resources table.

***Lentiviral transduction of organoids.*** Organoids were washed by PBS and dissociated into smaller clusters with TrypLE™ (Invitrogen, #12604-012) for 15 minutes at 37°C. Organoids were resuspended into 500 μL transduction solution containing 10 μM Y-27632 (Peprotech, #1293823), 8 μg/mL polybrene (Sigma, #107689) and concentrated lentivirus in organoid culture media. Spinoculation of resuspended organoids was performed at 800 g for 1 hour at 32°C. After spinoculation, organoids were incubated for 12-14 hours at 37°C and then replated onto a new 24-well plate.

***Immunoblotting.*** Western blot analyses were performed using standard method. Briefly, the pellet was lysed in RIPA buffer (150 mM NaCl, 1% Nonidet P-40, 0.5% deoxycholate, 0.1% SDS, 50 mM Tris-HCl at pH 7.5) with protease inhibitor cocktail (Roche, #04-693-124-001) and phosphatase inhibitor cocktail (Sigma, P5726). Protein concentration was measured by the BCA kit (Thermo Scientific, #23227). Cell lysates were separated by SDS Poly-acrylamide-gel-electrophoresis (Invitrogen, NP0323). PageRuler Plus Prestained Protein Ladder (Thermo Scientific, #26619) was used as molecular weight marker. Proteins were transferred to a PVDF membrane (Millipore, IPVH00010), blocked by 5% non-fat dry milk in 1X TBS buffer at pH 7.4 (Quality Biological, #351-086-151) with 0.05% Tween-20, and then probed with the indicated primary antibodies at 4°C overnight. Bound antibodies were visualized by chemiluminescence

(Thermo Scientific, #34580) using a horseradish peroxidase-conjugated secondary antibody and exposure of AccuRay blue X-Ray films (E&K Scientific, EK5129). Antibodies used for immunoblotting were listed in the key resources table.

***Immunohistochemistry and immunofluorescence staining.*** Organoids were fixed with 2% paraformaldehyde (Electron Microscopy Sciences, #15714) in PBS for 30 minutes at room temperature, washed with PBS twice, embedded in HistoGel™ (Thermo Scientific, HG-4000-012), and then transferred to 70% ethanol for paraffin-embedding. Organoids were sectioned at 5-mm thickness. Paraffin-embedded sections were deparaffinized and rehydrated before staining. For immunohistochemistry staining, antigen retrieval was achieved in sodium citrate buffer (10 μM sodium citrate at pH 6.0). Slides were incubated in 3% $H_2O_2$ solution (Fisher Scientific, H325-100) in methanol at room temperature for 10 minutes to block endogenous peroxidase activity. After washing, slides were blocked in Avidin/Biotin Solution (Vector Laboratories, SP2001) at room temperature for 30 minutes and then in blocking buffer (5% normal goat or donkey serum in PBS) for 1 hour. After blocking, slides were incubated with primary antibody in blocking buffer at 4°C overnight. Slides were washed by PBST (PBS with 0.05% Tween-20) and incubated with secondary antibody at room temperature for 30 minutes. Slides were washed by PBST and ABC reagent was applied (Vector Laboratories, PK-6101). After washing with PBST, DAB staining was performed for signal detection (Vector Laboratories, SK-4100). The slides were counterstained with hematoxylin (Sigma, MHS16) for 2 minutes and rinsed with water for 1 minute. Subsequent treatment with 1% acid alcohol 3 times to differentiate nuclear detail was performed along with sequential treatment with 0.2% ammonia for bluing, each of these steps were followed by a water rinse for 1 minute. Following this, the slides were rehydrated and mounted using mounting solution (Thermo Scientific, #4112).

For immunofluorescence staining, deparaffinization and rehydration procedures were as described above. Slides were blocked in blocking buffer at room temperature for 1 hour. After blocking, slides were incubated with primary antibody in blocking buffer at 4°C overnight. Slides

were washed by PBST and incubated with secondary antibody at room temperature for 30 minutes. After washes with PBST, slides were mounted by mounting solution with DAPI (Vector Laboratories, H-1500). Imaging was performed using fluorescence microscopy (Keyence, BZ-X700 series). For Alcian blue staining, slides were stained with Alcian blue (Thermo Fisher, #88043) following the manufacturer's instructions. Antibodies used for immunostaining were listed in the key resources table.

***Real-time quantitative PCR.*** Total RNA from organoids was isolated with the RNeasy kit (Qiagen, #74106). The on-column DNase digestion (Qiagen, #79254) was used to eliminate genomic DNA. A total of 0.5-1 μg RNA was used to synthesize complementary DNA using iScript™ Reverse Transcription Supermix (Bio-Rad, #1708841). Quantitative PCR was performed with Power SYBR™ Green PCR Master Mix (Thermo Scientific, #4368708). The primers used for quantitative PCR were listed in the key resources table.

***Cell proliferation and viability assay.*** Organoids were dissociated into smaller aggregates and single cells were sorted by FACS Aria II (BD Biosciences) as described above. A total of 20,000 cells were resuspended into 40μL Matrigel (R&D systems, Basement Membrane Extract type 2) and plated in a well of a 24-well plate. Over a period of 14 days, organoid growth was recorded daily by bright-field microscopy. YM-155 (Cayman Chemicals, #11490) was dissolved in DMSO. For 12-point full titration treatment of YM-155, a total of 5,000 cells were resuspended into 10 μL Matrigel and cultured in a well of a 96-well plate for 5 days before drug treatment. Cell viability was quantified 3 days after YM-155 treatment. For the cell viability assay, AlamarBlue™ Cell Viability Reagent (Invitrogen, DAL1100) in organoid culture media was added into the plate and incubated with organoids for 4 hours before being quantified using a Synergy H1 Hybrid Multi-mode Plate Reader (BioTek).

Author Manuscript Published OnlineFirst on January 15, 2021; DOI: 10.1158/2159-8290.CD-20-1109
Author manuscripts have been peer reviewed and accepted for publication but have not yet been edited.

***Luciferase assay.*** A total of 20,000 TOPflash mCherry-positive single cells were sorted by FACS Aria II (BD Biosciences) as described above. Cells were washed by PBS and the pellet was lysed in Passive Lysis Buffer (Promega, E194A). Firefly luciferase activities were measured using the Dual Luciferase Reporter Assay System (Promega, D1980).

***sgRNA design.*** Knockout sgRNA were designed using a combination of empirical data and on-target and off-target predictions. When available, empirical data from published CRISPR screens were used to pick the most active sgRNAs(78–80), otherwise the sgRNAs were designed as described previously(78). The sgRNA sequences used in this study are listed in the key resources table.

***High-throughput compound screening.*** Screening of the Emory Enriched Bioactive Library (EEBL), which includes 2,036 U.S. Food and Drug Administration (FDA) approved and bioactive compounds(81), was carried out using our miniaturized organoid culture platform in a 384-well format for HTS. Briefly, organoids grown in a 50 μl Matrigel droplet on a single well of a 24-well plate were harvested as described and re-suspended in ice-cold Matrigel (R&D systems, Basement Membrane Extract type 2) to form a cell/Matrigel mixture. 8 μL/well of the cells/Matrigel (~1,000 cells/well) mixture was dispensed onto a 384-well plate using a Multidrop Combi dispenser (Thermo Fisher Scientific). The plates were immediately centrifuged at 500 rpm for 1 min and incubated for 30 min at cell culture incubator to allow Matrigel solidification. 35 μL per well of organoid culture media was dispensed into the wells. The plates were sealed using gas permeable plate sealer (Breathe-Easy Sealing Film, Diversified Biotech, #BEM-1) and incubated for 5 days in cell culture incubator to allow organoid formation. Then, 0.1 μL of library compounds diluted in DMSO were added to each well using Pin-tool integrated with Beckman NX automated liquid handling system (Beckman Coulter, Danaher Corporation). The plates were centrifuged at 800 rpm for 5 min to ensure the uniform distribution of the compound into the wells. The final compound concentration was 4.6 μM and the final DMSO concentration was

0.2%. The plates were sealed with gas permeable plate sealer. After incubating with compound for 3 days, the viability of organoids was determined by CellTiter Blue reagent (Promega). Briefly, 5 μL of CellTiter Blue reagent was added to each well in 384-well plates using a MultiDrop Combi. After incubating at 37°C for 4 hours, the fluorescence intensity (FI), which is correlated with the number of viable cells, was measured using PHERAstar FSX multi-label plate reader (BMG LABTECH) with excitation at 540/20 nm and Emission at 590/20 nm.

***Data analysis for high throughput drug screening.*** Screening data were analyzed using CambridgeSoft Bioassay software. The performance of the organoids HTS viability assay in 384-well format was evaluated by Z' factor and Signal-to-background (S/B) ratio and were calculated as the following equations:

$Z' = 1 - (3SD_{DMSO\ control} + 3SD_{blank}) / (FI_{DMSO\ control} - FI_{blank})$

$S/B = FI_{DMSO\ control} / FI_{blank}$

Where $SD_{DMSO}$ and $SD_{blank}$ are the standard deviations, and $FI_{DMSO\ control}$ and $FI_{blank}$ are the corresponding average FI signal for the wells with DMSO control or blank with medium only without cells, respectively. A Z' factor between 0.5 and 1.0 indicating that the assay is robust for HTS(82). The effect of compound on the growth of organoids was expressed as % of control and calculated based on per plate as the following equations:

$\%\ of\ control = (FI\ compound - FI\ blank)/(FI_{DMSO\ control} - FI_{blank}) \times 100$

The dose-response effect of selected hit compounds from HTS on the growth of organoids was analyzed using GraphPad Prism 7 (GraphPad Software, Inc.).

***Master regulator analysis.*** The context-specific regulatory network used in this analysis was reverse-engineered from a collection of 200 gene expression profiles from STAD patients in TCGA(14) using the ARACNe algorithm(52). Specifically, ARACNe was used to infer regulatory targets of 1,813 transcription factors—including genes annotated in Gene Ontology molecular function database (GO) as 'transcription factor activity', 'DNA binding', 'transcription regulator

activity', or 'regulation of transcription' (GO:0003700, GO:0004677, GO:0030528, GO:0004677, GO: 0045449)—and a manually curated list of 969 transcriptional cofactors—including genes annotated as 'transcription cofactor activity', (GO:0003712, GO:0030528, GO:0045449). For each of these regulators, its protein activity was computed by VIPER(50) analysis of genes differentially expressed in *TP53/ARID1A* DKO compared to *TP53* KO samples, using the STAD-specific ARACNe regulatory network. The list of regulators and of their inferred differential activity in *TP53/ARID1A* DKO samples were then compared to the VIPER inferred protein activity profiles of all TCGA-STES patient samples, using the 'viperSimilarity' method of the VIPER package. This method computes the similarity between two samples based on the conservation of their differentially active proteins. This is accomplished by performing a gene set enrichment analysis of statistically significantly differentially active proteins in one context (e.g., *TP53/ARID1A* DKO) to protein differentially active in the other context (e.g. STES patients) and vice versa, using the aREA algorithm, an analytic extension of GSEA(83). The similarity scores obtained from viperSimilarity method are the z-scores of enrichment analysis. TCGA-STES samples and their subtype annotations were obtained from literature(84). The context-specific regulatory network of the TCGA-STES samples was reverse-engineered using ARACNe algorithm, and protein activity profiles of all samples were computed by VIPER analysis of genes differentially expressed in each TCGA-STES sample compared to the average gene expression in all samples, using STES specific ARACNe regulatory network.

***RNA-seq and data analysis.*** For the RNA-seq, two technical duplicates were included for each sample. RNA-seq libraries were generated by using NEBNext Ultra II Directional RNA Library Prep Kit coupled with Poly(A) mRNA Magnetic Isolation Module and NEBNext multiplex oligos for Illumina (New England Biolabs). The deep sequencing was performed on the NextSeq 500 sequencing system (Illumina) with 75-cycle, paired-end sequencing. RNA-seq data were aligned to hg38 human genome assembly using kallisto (v 0.44.0) with default parameters. Differential gene expression analysis was performed using DESeq2(85). Change in gene

expression between two conditions was defined as significant if |log2FC|>0.5 and adjusted p-value <0.05. ComplexHeatmap was used to produce heat maps(86).

***Somatic variant calling*.** Short reads produced by WGS on the Illumina platform were aligned to hg38 using BWA (v0.7.17). Following GATK (v4.1.4.1) best practice workflow(87), the raw alignment files (BAMs) were then pre-processed through marking duplicated reads and base recalibration. SNV and INDEL calls were made using MuTect2 in GATK package. The calls were then filtered and annotated using FilterMutectCalls and Funcotator in GATK. Somatic copy number aberrations (SCNAs) were estimated using CNVkit (v0.9.6)(88).

***Subcutaneous xenografts.*** NOD-scid IL2Rgamma$^{null}$ (NSG) immunodeficient mice were obtained from the Jackson Laboratory (#005557). For xenograft studies, male adult NSG mice (~8-10 weeks old) were randomly divided into experimental groups. Mice were subcutaneously injected with organoids (1.5 x $10^6$ cells in 150 μL 100% Matrigel per injection). Mice were sacrificed 3 months after inoculation of organoids. All mouse studies were approved by the Stanford Institutional Animal Care and Use Committee (IACUC).

***Data availability.*** The datasets generated in this study are available from the corresponding author on reasonable request. Raw and processed sequencing data were deposited into the Gene Expression Omnibus (GEO) under accession code GSE164179.

## References

1. Flavahan WA, Gaskell E, Bernstein BE. Epigenetic plasticity and the hallmarks of cancer. Science. 2017;357:eaal2380.
2. Hodges C, Kirkland JG, Crabtree GR. The many roles of BAF (mSWI/SNF) and PBAF complexes in cancer. Cold Spring Harb Perspect Med. 2016;6:a026930.
3. Mashtalir N, D'Avino AR, Michel BC, Luo J, Pan J, Otto JE, et al. Modular Organization and Assembly of SWI/SNF Family Chromatin Remodeling Complexes. Cell. 2018;175:1272–88.
4. Wu JI, Lessard J, Crabtree GR. Understanding the Words of Chromatin Regulation. Cell. 2009;136:200–6.
5. Ho L, Crabtree GR. Chromatin remodelling during development. Nature. 2010;463:474–84.
6. Pulice JL, Kadoch C. Composition and function of mammalian SWI/SNF chromatin remodeling complexes in human disease. Cold Spring Harb Symp Quant Biol. 2016;81:53–60.
7. Dykhuizen EC, Hargreaves DC, Miller EL, Cui K, Korshunov A, Kool M, et al. BAF complexes facilitate decatenation of DNA by topoisomerase IIα. Nature. 2013;497:624–7.
8. Kadoch C, Hargreaves DC, Hodges C, Elias L, Ho L, Ranish J, et al. Proteomic and bioinformatic analysis of mammalian SWI/SNF complexes identifies extensive roles in human malignancy. Nat Genet. 2013;45:592–601.
9. Kadoch C, Crabtree GR. Reversible disruption of mSWI/SNF (BAF) complexes by the SS18-SSX oncogenic fusion in synovial sarcoma. Cell. 2013;153:71–85.
10. Wilson BG, Wang X, Shen X, McKenna ES, Lemieux ME, Cho YJ, et al. Epigenetic antagonism between polycomb and SWI/SNF complexes during oncogenic transformation. Cancer Cell. 2010;18:316–28.
11. McBride MJ, Pulice JL, Beird HC, Ingram DR, D'Avino AR, Shern JF, et al. The SS18-SSX Fusion Oncoprotein Hijacks BAF Complex Targeting and Function to Drive Synovial Sarcoma. Cancer Cell. 2018;33:1128–41.
12. Wu JN, Roberts CWM. ARID1A mutations in cancer: Another epigenetic tumor suppressor? Cancer Discov. 2013;3:35–43.
13. Zang ZJ, Cutcutache I, Poon SL, Zhang SL, Mcpherson JR, Tao J, et al. Exome sequencing of gastric adenocarcinoma identifies recurrent somatic mutations in cell adhesion and chromatin remodeling genes. Nat Genet. 2012;44:570–4.
14. Bass AJ, Thorsson V, Shmulevich I, Reynolds SM, Miller M, Bernard B, et al. Comprehensive molecular characterization of gastric adenocarcinoma. Nature. 2014;513:202–9.
15. Cristescu R, Lee J, Nebozhyn M, Kim KM, Ting JC, Wong SS, et al. Molecular analysis of gastric cancer identifies subtypes associated with distinct clinical outcomes. Nat Med. 2015;21:449–56.
16. Chandler RL, Brennan J, Schisler JC, Serber D, Patterson C, Magnuson T. ARID1a-DNA Interactions Are Required for Promoter Occupancy by SWI/SNF. Mol Cell Biol. 2013;33:265–80.
17. Gao X, Tate P, Hu P, Tjian R, Skarnes WC, Wang Z. ES cell pluripotency and germ-layer formation require the SWI/SNF chromatin remodeling component BAF250a. Proc Natl Acad Sci U S A. 2008;105:6656–61.
18. Chandler RL, Damrauer JS, Raab JR, Schisler JC, Wilkerson MD, Didion JP, et al. Coexistent ARID1A-PIK3CA mutations promote ovarian clear-cell tumorigenesis through pro-tumorigenic inflammatory cytokine signalling. Nat Commun. 2015;27:6118.
19. Mathur R, Alver BH, San Roman AK, Wilson BG, Wang X, Agoston AT, et al. ARID1A loss impairs enhancer-mediated gene regulation and drives colon cancer in mice. Nat Genet. 2017;49:296–302.
20. Hiramatsu Y, Fukuda A, Ogawa S, Goto N, Ikuta K, Tsuda M, et al. Arid1a is essential for

intestinal stem cells through Sox9 regulation. Proc Natl Acad Sci U S A. 2019;116:1704–13.

21. Wilson MR, Reske JJ, Holladay J, Wilber GE, Rhodes M, Koeman J, et al. ARID1A and PI3-kinase pathway mutations in the endometrium drive epithelial transdifferentiation and collective invasion. Nat Commun. 2019;10:3554.
22. Kimura Y, Fukuda A, Ogawa S, Maruno T, Takada Y, Tsuda M, et al. ARID1A Maintains Differentiation of Pancreatic Ductal Cells and Inhibits Development of Pancreatic Ductal Adenocarcinoma in Mice. Gastroenterology. 2018;155:194–209.
23. Wang W, Friedland SC, Guo B, O'Dell MR, Alexander WB, Whitney-Miller CL, et al. ARID1A, a SWI/SNF subunit, is critical to acinar cell homeostasis and regeneration and is a barrier to transformation and epithelial-mesenchymal transition in the pancreas. Gut. 2019;68:1245–58.
24. Wang SC, Nassour I, Xiao S, Zhang S, Luo X, Lee J, et al. SWI/SNF component ARID1A restrains pancreatic neoplasia formation. Gut. 2019;68:1259–70.
25. Livshits G, Alonso-Curbelo D, Morris JP, Koche R, Saborowski M, Wilkinson JE, et al. Arid1a restrains Kras-dependent changes in acinar cell identity. Elife. 2018;7:e35216.
26. Sun X, Wang SC, Wei Y, Luo X, Jia Y, Li L, et al. Arid1a Has Context-Dependent Oncogenic and Tumor Suppressor Functions in Liver Cancer. Cancer Cell. 2017;32:574–89.
27. Han L, Madan V, Mayakonda A, Dakle P, Woon TW, Shyamsunder P, et al. Chromatin remodeling mediated by ARID1A is indispensable for normal hematopoiesis in mice. Leukemia. 2019;33:2291–305.
28. Lo Y-H, Karlsson K, Kuo CJ. Applications of organoids for cancer biology and precision medicine. Nat Cancer. 2020;1:761–773.
29. Li X, Nadauld L, Ootani A, Corney DC, Pai RK, Gevaert O, et al. Oncogenic transformation of diverse gastrointestinal tissues in primary organoid culture. Nat Med. 2014;20:769–77.
30. Matano M, Date S, Shimokawa M, Takano A, Fujii M, Ohta Y, et al. Modeling colorectal cancer using CRISPR-Cas9-mediated engineering of human intestinal organoids. Nat Med. 2015;21:256–62.
31. Drost J, Van Jaarsveld RH, Ponsioen B, Zimberlin C, Van Boxtel R, Buijs A, et al. Sequential cancer mutations in cultured human intestinal stem cells. Nature. 2015;521:43–7.
32. Nanki K, Toshimitsu K, Takano A, Fujii M, Shimokawa M, Ohta Y, et al. Divergent Routes toward Wnt and R-spondin Niche Independency during Human Gastric Carcinogenesis. Cell. 2018;174:856–69.
33. Ho L, Ronan JL, Wu J, Staahl BT, Chen L, Kuo A, et al. An embryonic stem cell chromatin remodeling complex, esBAF, is essential for embryonic stem cell self-renewal and pluripotency. Proc Natl Acad Sci U S A. 2009;106:5181–6.
34. Bartfeld S, Bayram T, Van De Wetering M, Huch M, Begthel H, Kujala P, et al. In vitro expansion of human gastric epithelial stem cells and their responses to bacterial infection. Gastroenterology. 2015;148:126–36.
35. Fujii M, Clevers H, Sato T. Modeling Human Digestive Diseases With CRISPR-Cas9–Modified Organoids. Gastroenterology. 2019;156:562–76.
36. Uhler C, Shivashankar G V. Nuclear Mechanopathology and Cancer Diagnosis. Trends in Cancer. 2018;4:320–31.
37. Webster M, Wikin KL, Cohen-Fix O. Sizing up the nucleus: Nuclear shape, size and nuclear-envelope assembly. J Cell Sci. 2009;122:1477–86.
38. Tan P, Yeoh KG. Genetics and Molecular Pathogenesis of Gastric Adenocarcinoma. Gastroenterology. 2015;149:1153–62.
39. Mills JC, Shivdasani RA. Gastric epithelial stem cells. Gastroenterology. 2011;140:412–24.
40. Hayakawa Y, Fox JG, Wang TC. The Origins of Gastric Cancer From Gastric Stem Cells:

Lessons From Mouse Models. CMGH. 2017;3:331–8.
41. Giroux V, Rustgi AK. Metaplasia: Tissue injury adaptation and a precursor to the dysplasia-cancer sequence. Nat Rev Cancer. 2017;17:594–604.
42. Petersen CP, Mills JC, Goldenring JR. Murine Models of Gastric Corpus Preneoplasia. CMGH. 2017;3:11–26.
43. Stange DE, Koo BK, Huch M, Sibbel G, Basak O, Lyubimova A, et al. Differentiated Troy+ chief cells act as reserve stem cells to generate all lineages of the stomach epithelium. Cell. 2013;155:357–68.
44. Wang XT, Kong FB, Mai W, Li L, Pang LM. MUC1 immunohistochemical expression as a prognostic factor in gastric cancer: Meta-analysis. Dis Markers. 2016;9421571:1–8.
45. Barriga FM, Montagni E, Mana M, Mendez-Lago M, Hernando-Momblona X, Sevillano M, et al. Mex3a Marks a Slowly Dividing Subpopulation of Lgr5+ Intestinal Stem Cells. Cell Stem Cell. 2017;20:801–16.
46. Yan KS, Gevaert O, Zheng GXY, Anchang B, Probert CS, Larkin KA, et al. Intestinal Enteroendocrine Lineage Cells Possess Homeostatic and Injury-Inducible Stem Cell Activity. Cell Stem Cell. 2017;21:78–90.
47. Horst D, Gu X, Bhasin M, Yang Q, Verzi M, Lin D, et al. Requirement of the epithelium-specific Ets transcription factor Spdef for mucous gland cell function in the gastric antrum. J Biol Chem. 2010;285:35047–55.
48. Gregorieff A, Stange DE, Kujala P, Begthel H, van den Born M, Korving J, et al. The Ets-Domain Transcription Factor Spdef Promotes Maturation of Goblet and Paneth Cells in the Intestinal Epithelium. Gastroenterology. 2009;137:1333–45.
49. Noah TK, Kazanjian A, Whitsett J, Shroyer NF. SAM pointed domain ETS factor (SPDEF) regulates terminal differentiation and maturation of intestinal goblet cells. Exp Cell Res. 2010;316:452–65.
50. Alvarez MJ, Shen Y, Giorgi FM, Lachmann A, Ding BB, Hilda Ye B, et al. Functional characterization of somatic mutations in cancer using network-based inference of protein activity. Nat Genet. 2016;48:838–47.
51. Califano A, Alvarez MJ. The recurrent architecture of tumour initiation, progression and drug sensitivity. Nat Rev Cancer. 2017;17:116–30.
52. Basso K, Margolin AA, Stolovitzky G, Klein U, Dalla-Favera R, Califano A. Reverse engineering of regulatory networks in human B cells. Nat Genet. 2005;37:382–90.
53. Wierstra I. FOXM1 (Forkhead box M1) in tumorigenesis. Overexpression in human cancer, implication in tumorigenesis, oncogenic functions, tumor-suppressive properties, and target of anticancer therapy. Adv Cancer Res. 2013;119:191–419.
54. Yan HHN, Siu HC, Law S, Ho SL, Yue SSK, Tsui WY, et al. A Comprehensive Human Gastric Cancer Organoid Biobank Captures Tumor Subtype Heterogeneity and Enables Therapeutic Screening. Cell Stem Cell. 2018;23:882–97.
55. Bitler BG, Wu S, Park PH, Hai Y, Aird KM, Wang Y, et al. ARID1A-mutated ovarian cancers depend on HDAC6 activity. Nat Cell Biol. 2017;19:962–73.
56. Fukumoto T, Park PH, Wu S, Fatkhutdinov N, Karakashev S, Nacarelli T, et al. Repurposing Pan-HDAC Inhibitors for ARID1A-Mutated Ovarian Cancer. Cell Rep. 2018;22:3393–400.
57. Lee D, Yu EJ, Ham IH, Hur H, Kim YS. AKT inhibition is an effective treatment strategy in ARID1A-deficient gastric cancer cells. Onco Targets Ther. 2017;10:4153–9.
58. Samartzis EP, Gutsche K, Dedes KJ, Fink D, Stucki M, Imesch P. Loss of ARID1A expression sensitizes cancer cells to PI3K- and AKT-inhibition. Oncotarget. 2014;5:5295–303.
59. Nakahara T, Takeuchi M, Kinoyama I, Minematsu T, Shirasuna K, Matsuhisa A, et al. YM155, a novel small-molecule survivin suppressant, induces regression of established human hormone-refractory prostate tumor xenografts. Cancer Res. 2007;67:8014–21.
60. Altieri DC. Validating survivin as a cancer therapeutic target. Nat Rev Cancer. 2003;3:46–54.

61. Wheatley SP, Altieri DC. Survivin at a glance. J Cell Sci. 2019;132:jcs223826.
62. Drost J, Van Boxtel R, Blokzijl F, Mizutani T, Sasaki N, Sasselli V, et al. Use of CRISPR-modified human stem cell organoids to study the origin of mutational signatures in cancer. Science. 2017;358:234–8.
63. Lee J, Snyder ER, Liu Y, Gu X, Wang J, Flowers BM, et al. Reconstituting development of pancreatic intraepithelial neoplasia from primary human pancreas duct cells. Nat Commun. 2017;8:14686.
64. Seino T, Kawasaki S, Shimokawa M, Tamagawa H, Toshimitsu K, Fujii M, et al. Human Pancreatic Tumor Organoids Reveal Loss of Stem Cell Niche Factor Dependence during Disease Progression. Cell Stem Cell. 2018;22:454–67.
65. Dekkers JF, Whittle JR, Vaillant F, Chen H-R, Dawson C, Liu K, et al. Modeling Breast Cancer Using CRISPR-Cas9–Mediated Engineering of Human Breast Organoids. JNCI J Natl Cancer Inst. 2019;112:540–4.
66. Artegiani B, van Voorthuijsen L, Lindeboom RGH, Seinstra D, Heo I, Tapia P, et al. Probing the Tumor Suppressor Function of BAP1 in CRISPR-Engineered Human Liver Organoids. Cell Stem Cell. 2019;24:927–43.
67. Chen K, Yang D, Li X, Sun B, Song F, Cao W, et al. Mutational landscape of gastric adenocarcinoma in Chinese: Implications for prognosis and therapy. Proc Natl Acad Sci U S A. 2015;112:1107–12.
68. Sigal M, Logan CY, Kapalczynska M, Mollenkopf HJ, Berger H, Wiedenmann B, et al. Stromal R-spondin orchestrates gastric epithelial stem cells and gland homeostasis. Nature. 2017;548:451–5.
69. Barker N, Huch M, Kujala P, van de Wetering M, Snippert HJ, van Es JH, et al. Lgr5+ve Stem Cells Drive Self-Renewal in the Stomach and Build Long-Lived Gastric Units In Vitro. Cell Stem Cell. 2010;6:25–36.
70. Lo YH, Noah TK, Chen MS, Zou W, Borras E, Vilar E, et al. SPDEF Induces Quiescence of Colorectal Cancer Cells by Changing the Transcriptional Targets of β-catenin. Gastroenterology. 2017;153:205–18.
71. Noah TK, Lo YH, Price A, Chen G, King E, Washington MK, et al. SPDEF functions as a colorectal tumor suppressor by inhibiting β-catenin activity. Gastroenterology. 2013;144:1012–23.
72. Kim KH, Kim W, Howard TP, Vazquez F, Tsherniak A, Wu JN, et al. SWI/SNF-mutant cancers depend on catalytic and non-catalytic activity of EZH2. Nat Med. 2015;21:1491–6.
73. Bitler BG, Aird KM, Garipov A, Li H, Amatangelo M, Kossenkov A V., et al. Synthetic lethality by targeting EZH2 methyltransferase activity in ARID1A-mutated cancers. Nat Med. 2015;21:231–8.
74. Ogiwara H, Takahashi K, Sasaki M, Kuroda T, Yoshida H, Watanabe R, et al. Targeting the Vulnerability of Glutathione Metabolism in ARID1A-Deficient Cancers. Cancer Cell. 2019;35:177–90.
75. Han K, Pierce SE, Li A, Spees K, Anderson GR, Seoane JA, et al. CRISPR screens in cancer spheroids identify 3D growth-specific vulnerabilities. Nature. 2020;580:136–41.
76. Chen B, Gilbert LA, Cimini BA, Schnitzbauer J, Zhang W, Li GW, et al. Dynamic imaging of genomic loci in living human cells by an optimized CRISPR/Cas system. Cell. 2013;155:1479–91.
77. Horlbeck MA, Gilbert LA, Villalta JE, Adamson B, Pak RA, Chen Y, et al. Compact and highly active next-generation libraries for CRISPR-mediated gene repression and activation. Elife. 2016;5:e19760.
78. Doench JG, Fusi N, Sullender M, Hegde M, Vaimberg EW, Donovan KF, et al. Optimized sgRNA design to maximize activity and minimize off-target effects of CRISPR-Cas9. Nat Biotechnol. 2016;34:184–91.
79. Sanson KR, Hanna RE, Hegde M, Donovan KF, Strand C, Sullender ME, et al. Optimized libraries for CRISPR-Cas9 genetic screens with multiple modalities. Nat Commun. 2018;9:5416.

80. Wang T, Wei JJ, Sabatini DM, Lander ES. Genetic screens in human cells using the CRISPR-Cas9 system. Science. 2014;343:80–4.
81. Mo X, Tang C, Niu Q, Ma T, Du Y, Fu H. HTiP: High-Throughput Immunomodulator Phenotypic Screening Platform to Reveal IAP Antagonists as Anti-cancer Immune Enhancers. Cell Chem Biol. 2019;26:331–9.
82. Zhang JH, Chung TDY, Oldenburg KR. A simple statistical parameter for use in evaluation and validation of high throughput screening assays. J Biomol Screen. 1999;4:67–73.
83. Subramanian A, Tamayo P, Mootha VK, Mukherjee S, Ebert BL, Gillette MA, et al. Gene set enrichment analysis: A knowledge-based approach for interpreting genome-wide expression profiles. Proc Natl Acad Sci U S A. 2005;102:15545–50.
84. Liu Y, Sethi NS, Hinoue T, Schneider BG, Cherniack AD, Sanchez-Vega F, et al. Comparative Molecular Analysis of Gastrointestinal Adenocarcinomas. Cancer Cell. 2018;33:721–35.
85. Love MI, Huber W, Anders S. Moderated estimation of fold change and dispersion for RNA-seq data with DESeq2. Genome Biol. 2014;15:550.
86. Gu Z, Eils R, Schlesner M. Complex heatmaps reveal patterns and correlations in multidimensional genomic data. Bioinformatics. 2016;32:2847–9.
87. Depristo MA, Banks E, Poplin R, Garimella K V., Maguire JR, Hartl C, et al. A framework for variation discovery and genotyping using next-generation DNA sequencing data. Nat Genet. 2011;43:491–8.
88. Talevich E, Shain AH, Botton T, Bastian BC. CNVkit: Genome-Wide Copy Number Detection and Visualization from Targeted DNA Sequencing. PLoS Comput Biol. 2016;12:e1004873.

Author Manuscript Published OnlineFirst on January 15, 2021; DOI: 10.1158/2159-8290.CD-20-1109
Author manuscripts have been peer reviewed and accepted for publication but have not yet been edited.

## Figure Legends

**Figure 1. Establishment of clonal *TP53/ARID1A* knockout human gastric organoid lines.** **A**, The *TP53* indel created by CRISPR/Cas9 cleavage was determined by Sanger sequencing. **B**, Establishment of a stable Cas9-expressing engineered *TP53* KO human gastric organoid line. After antibiotic (Blasticidin) selection, Cas9 expression was confirmed by immunoblot analysis. **C**, Highly efficient CRISPR/Cas9 cleavage in Cas9-expressing *TP53* KO organoids. A lentiviral construct containing a GFP guide RNA targeting the GFP reporter in the same construct was delivered into control *TP53* KO and the Cas9-expressing *TP53* KO organoids. After antibiotic (Puromycin) selection, GFP-positive cells were quantified by flow cytometry. **D**, Five different *TP53/ARID1A* DKO clones were established. *ARID1A* indels were determined by Sanger sequencing. **E**, Immunoblot analysis of ARID1A and ARID1B expression. **F**, IHC staining of ARID1A in *TP53* KO versus *TP53/ARID1A* DKO organoids.

**Figure 2. CRISPR KO of *ARID1A* promotes gastric malignancy.** **A**, *TP53* KO (control) organoids were typically well-organized morphologically; however, *TP53/ARID1A* DKO organoids exhibited different degrees of architectural complexity. H&E staining. Quantitation revealed increased epithelial stratification (green bar), structural complexity (blue bar), and loss of polarity (red bar) in all five *TP53/ARID1A* DKO clones. **B**, Immunofluorescence staining of the apical-specific marker ZO1 (red) showed disruptions in apicobasal polarity in a subset of *TP53*/*ARID1A* DKO organoid cells. The arrow (orange) indicates loss of polarity with inappropriate basolateral ZO1 expression. Cell membrane was stained with CTNNB1 (green). Nuclei were stained with DAPI (blue). **C**, *ARID1A*-deficient organoids exhibit hyperproliferation. *TP53* KO and *TP53*/*ARID1A* DKO organoids were grown from 20,000 single FACS-sorted BFP+ cells. Brightfield images were taken after cell sorting. Quantification of organoid size is shown (n=400 per group). **D**, Quantification of EdU-positive proliferating cells in *TP53* KO and *TP53*/*ARID1A* DKO organoids from independent experiments (N=3) at day 6 after passage. **E**,

Quantification of metabolic activity from independent experiments (N=6) was determined by Alamar blue assay at day 12 after passage. Relative metabolic activity was normalized to *TP53* KO organoids (Control). Dots indicate independent experiments. The horizontal bar indicates mean. The error bar represents SEM. *$P$<0.05, ***$P$<0.005. ns, not significant. **F**, *ARID1A*-deficient organoids exhibited efficient *in* vivo tumor formation upon subcutaneous xenografting into NSG mice. *TP53/ARID1A* DKO xenografts formed larger tumors compare with *TP53* KO xenografts. H&E staining. **G**, A significant negative correlation between ARID1A expression and tumor grade was identified in a human gastric cancer tissue microarray (total 197 patients). ARID1A expression was assessed by IHC.

**Figure 3. *ARID1A* knockout induces mucinous metaplasia. A**, Schematic illustration of gastric epithelium. Different cell lineages and specific lineage markers are indicated. **B**, Western blot of mucin-producing pit cell and mucous neck cell markers, TFF1, TFF2 and LYZ, reveals upregulation in *TP53/ARID1A* DKO organoids. Quantification of expression from independent experiments (N>3) was shown. Dots indicate independent experiments. **C**, Immunofluorescence staining of MUC5AC (green) and TFF1 (red) in engineered organoids and the donor primary gastric tissues. Nuclei were stained with DAPI (blue). Quantification of MUC5AC-positive organoids is shown. **D**, Mucin production in engineered organoids and donor primary gastric tissues detected by Alcian blue staining. Nuclei were counterstained by nuclear fast red. Quantification of Alcian blue-positive organoids indicate increased mucin in all five *TP53/ARID1A* DKO organoids lines. **E**, *TP53/ARID1A* DKO xenografts in a subcutaneously xenografted NSG mice retain their mucin-secreting phenotype *in vivo*. Alcian blue and PAS staining. Goblet-like (Alcian blue -positive) and pit-like (PAS positive) cells were indicated. **F**, Quantification of mitotic cells. Goblet-like and pit-like cells with mitotic figures were shown. H&E staining. **G**, Immunofluorescence staining of *TP53/ARID1A* DKO organoids showing LYZ-positive (red) or MUC5-positive (red) proliferating cells (KI67+, green). **H,** IHC staining of CDX2 in xenografts and the donor primary gastric tissues. Colon tissues were used as positive control.

Author Manuscript Published OnlineFirst on January 15, 2021; DOI: 10.1158/2159-8290.CD-20-1109
Author manuscripts have been peer reviewed and accepted for publication but have not yet been edited.

**I,** IHC staining of MUC2 in organoids, xenografts and the donor primary gastric tissues. Colon tissues were used as positive control. **J,** Immunofluorescence staining of CLDN18 (white), MUC6 (red) and PGC (green) in *TP53/ARID1A* DKO organoids, xenografts and the donor primary gastric tissues. Cells within SPEM features (MUC6 and PGC double positive) are marked by arrows. **K**, A significant negative correlation between ARID1A (brown) IHC expression and mucin (blue, Alcian blue) production was identified in a human gastric cancer tissue microarray (total 197 patients).

**Figure 4. Loss of *ARID1A* inhibits canonical Wnt/β-catenin activity.** **A**, Wnt/β-catenin-induced activity was decreased in *TP53/ARID1A* DKO organoids infected by lentivirus containing TOPflash Wnt reporter and mCherry followed by luciferase assay on 20,000 sorted mCherry-positive cells. Quantification of luciferase activity from independent experiments (N=5) is shown. Luciferase activity was normalized to *TP53* KO organoids (Control). **B**, The mucin-producing phenotype was genetically rescued by lentiviral expression of an N-terminal truncated gain-of-function β-catenin mutant (*CTNNB1*ΔN90). After virus transduction and antibiotic (Neomycin) selection, protein expression in the engineered organoids was analyzed by Western blot as indicated. **C**, Immunofluorescence staining of apically-restricted transmembrane MUC1 (green) and membrane protein CDH1 (red) demonstrates that *CTNNB1*ΔN90 reduces mucin production and architectural complexity of *TP53/ARID1A* DKO organoids. **D**, Venn diagram indicates overlap of genes that are significantly increased (101 genes) or decreased (143 genes) at least 2-fold in organoids with *CTNNB1*ΔN90 alleles. **E**, Gene ontology analysis identified top key terms significantly associated with transcriptional profiles in *CTNNB1*ΔN90 organoids. **F**, Wnt/β-catenin target genes were upregulated in *CTNNB1*ΔN90 organoids. **G**, Gastric mucous cell and intestinal goblet cell markers were significantly downregulated in *CTNNB1*ΔN90 organoids. The expression of transcription factors *SPDEF*, *SOX21*, *THRB*, *SIX2* was shown. **H**, Phenotypic changes induced by *ARID1A* loss were partially restored by lentivirus *CTNNB1*ΔN90.

Author Manuscript Published OnlineFirst on January 15, 2021; DOI: 10.1158/2159-8290.CD-20-1109
Author manuscripts have been peer reviewed and accepted for publication but have not yet been edited.

H&E staining and brightfield images. Relative stratification was quantified by counting the number of cells per length of perimeter of individual organoids. **I**, Constitutive Wnt signaling activation by *CTNNB1*ΔN90 did not rescue *ARID1A* KO-mediated proliferation. Single cells (20,000/40 μL Matrigel) from *TP53* KO and *TP53*/*ARID1A* DKO organoids with and without lentivirus *CTNNB1*ΔN90 underwent Alamar blue quantification of cell viability at day 12. Relative cell viability was normalized to control *TP53* KO organoids (Control). Three independent experiments (N=3) were performed. In A, H and I, dots indicate independent experiments, horizontal bars indicate mean and error bars represent SEM. **P*<0.05, ****P*<0.005. ns, not significant.

**Figure 5. *ARID1A* loss-associated gene master regulatory modules identify a *FOXM1/BIRC5* node and recapitulate TCGA MSI and EBV human gastric cancers. A,** Heatmap of significant differentially expressed genes with at least 2-fold change in each *TP53/ARID1A* DKO lines, compared with *TP53* KO control line. A total of 412 up-regulated genes and 675 down-regulated genes were identified. Selected genes and signaling pathways are listed. **B**, Gene ontology analysis identified top key terms significantly associated with transcriptional profiles in *TP53/ARID1A* DKO organoids. **C**, Top 10 master regulators from ARACNe and VIPER prediction that were activated in *TP53/ARID1A* DKO organoids versus control *TP53* KO are reported. Several FOXM1 targets, including *BIRC5, CKS1B, CDC25C, CCNB1, CCNB2, CDK1*, *AURKA* and *AURKB* were significantly upregulated in *ARID1A*-deficient cells. **D**, Western immunoblotting analysis demonstrated that FOXM1 targets, BIRC5 and AURKB, were upregulated in *TP53/ARID1A* DKO organoids. Quantification of BIRC5 and AURKB expression from independent experiments (N>3) was shown. Dots indicate independent experiments. The horizontal bar indicates mean. The error bar represents SEM. **E**, Comparison of master transcriptional regulators in *ARID1A* KO organoids to TCGA STAD gastric cancer patient cases indicated significant similarities between organoids and TCGA MSI and EBV subtypes. The p-value computed by t-test (one sample) with the alternative hypothesis of true

mean of the similarity score is greater than zero. Red and blue colors indicate high and low similarity concurrence, respectively. **F**, Comparison of master transcriptional regulators in *ARID1A*-deficient organoids to gastric cancer patient-derived organoids (PDOs) indicated significant similarities between engineered *TP53/ARID1A* DKO organoids and MSI subtype PDOs.

**Figure 6. *ARID1A* deletion confers therapeutic vulnerability to BIRC5/survivin inhibition.** **A**, High-throughput small molecule and bioactive screening in engineered organoids. **B**, Histogram of high-throughput screening of an FDA-approved small molecule compound library (2,036 compounds) in *TP53/ARID1A* DKO organoids. Organoids were dissociated into smaller clusters, re-plated into 384-well plates, and cultured for 5 days before drug treatment. Cell viability was quantified 3 days after compound treatment. The signal-to-background (S/B) ratio and Z' indicated robust assay performance. The top 50 primary hits are indicated below the dashed red line and were selected for counter screening. **C**, YM-155, a BIRC5/survivin inhibitor, exhibited *ARID1A*-specific synthetic lethality. Fully-titrated counter screening for YM-155 was performed in two *TP53* KO lines versus five additional *TP53/ARID1A* DKO clones. **D**, Brightfield images after organoid treatment with YM-155 ($IC_{50}$, 0.03 μM) for 3 days. YM-155 selectively inhibited growth of *TP53/ARID1A* DKO but not *TP53* KO organoids. **E**, Establishment of stable BIRC5 over-expressing *BIRC5/TP53* KO and *BIRC5/TP53/ARID1A* DKO organoid lines. After antibiotic (Neomycin) selection, BIRC5 expression was confirmed by immunoblot analysis. **F**, Constitutive expression of BIRC5 rescued the YM-155-associated sensitivity in *TP53/ARID1A* DKO organoids. Organoids were treated with YM-155 ($IC_{50}$, 0.03 μM) for 3 days. Three independent experiments (N=3) were performed. **G**, YM-155 treatment did not alter mucin production in *TP53/ARID1A* DKO organoids. Alcian blue staining. Nuclei were counterstained by nuclear fast red. **H**, Western immunoblotting analysis indicated that a gain-of-function β-catenin mutant (*CTNNB1*ΔN90) was sufficient to induce Wnt/β-catenin targets, LEF1 and TCF1; however, YM-155 treatment did not affect Wnt/β-catenin activity. **I**, YM-155 $IC_{50}$

Author Manuscript Published OnlineFirst on January 15, 2021; DOI: 10.1158/2159-8290.CD-20-1109
Author manuscripts have been peer reviewed and accepted for publication but have not yet been edited.

treatment (0.03 μM) did not affect Wnt/β-catenin-induced TOPflash reporter activity. Quantification of luciferase activity from independent experiments (N=4) is shown. Luciferase activity was normalized to DMSO treatment. A gain-of-function β-catenin mutant (*CTNNB1*ΔN90) organoid line was used as the positive control. **J**, Lentiviral expression of *CTNNB1*ΔN90 did not rescue the BIRC5 expression, Western blot. **K**, Lentiviral expression of *CTNNB1*ΔN90 did not rescue the selective YM-155 sensitivity of *ARID1A*-deficient cells. Fully-titrated YM-155 treatment was performed in *TP53* KO versus *TP53/ARID1A* DKO and *TP53/ARID1A* DKO plus *CTNNB1*ΔN90 organoid clones. Alamar blue, three independent experiments (N=3).

**Figure 7. Model of *ARID1A* loss-mediated oncogenic transformation in early human gastric cancer.** *ARID1A* loss induces functionally independent transformation pathways during early gastric tumorigenesis in which non-essential Wnt-regulated mucinous differentiation operates in parallel with versus essential YM-155-sensitive FOXM1/BIRC5-regulated cell proliferation.

# Figure 1

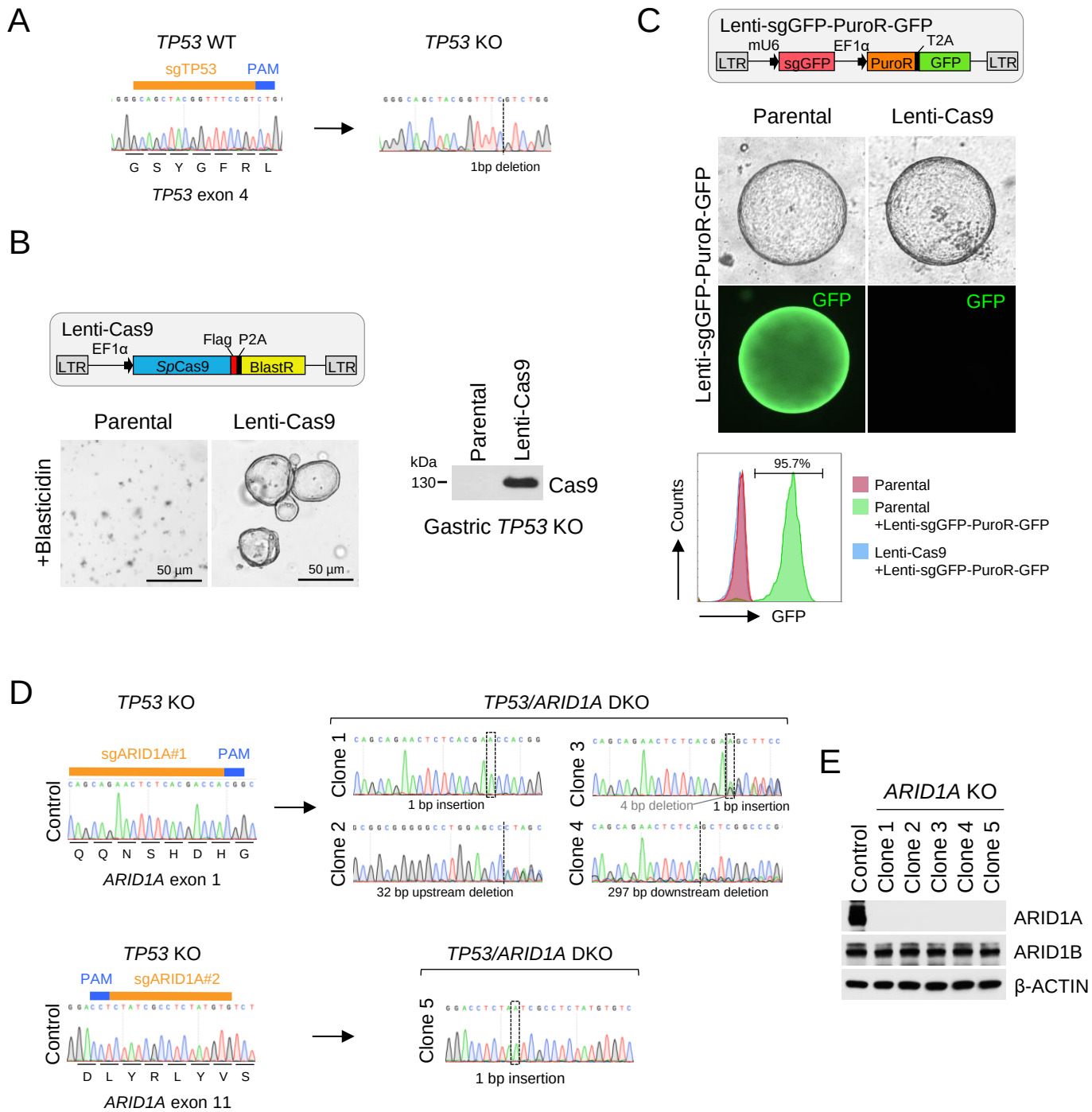

# Figure 2

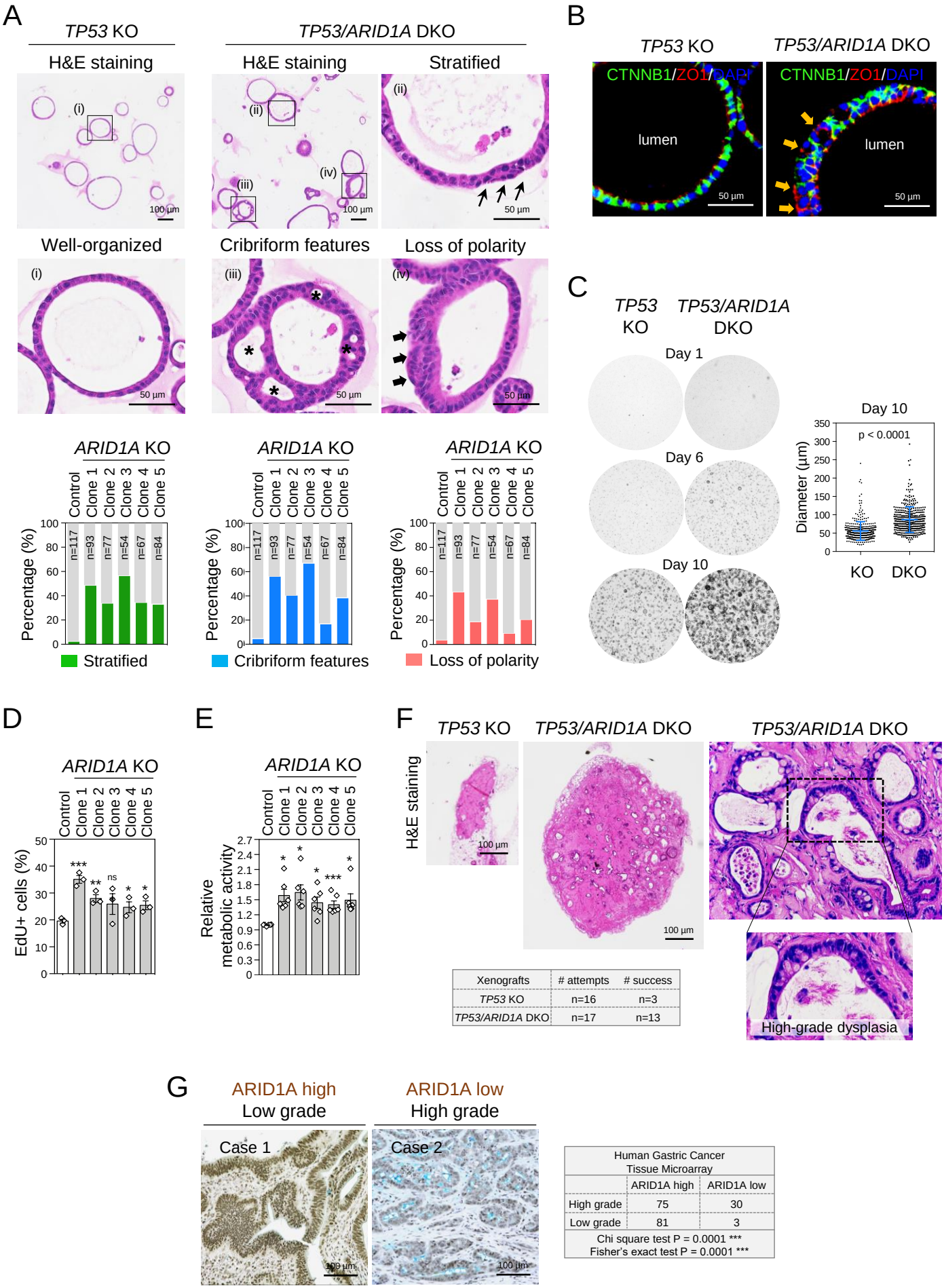


| Xenografts | # attempts | # success |
|---|---|---|
| *TP53* KO | n=16 | n=3 |
| *TP53/ARID1A* DKO | n=17 | n=13 |

| Human Gastric Cancer Tissue Microarray | | |
|---|---|---|
| | ARID1A high | ARID1A low |
| High grade | 75 | 30 |
| Low grade | 81 | 3 |
| Chi square test P = 0.0001 *** | | |
| Fisher's exact test P = 0.0001 *** | | |

# Figure 3

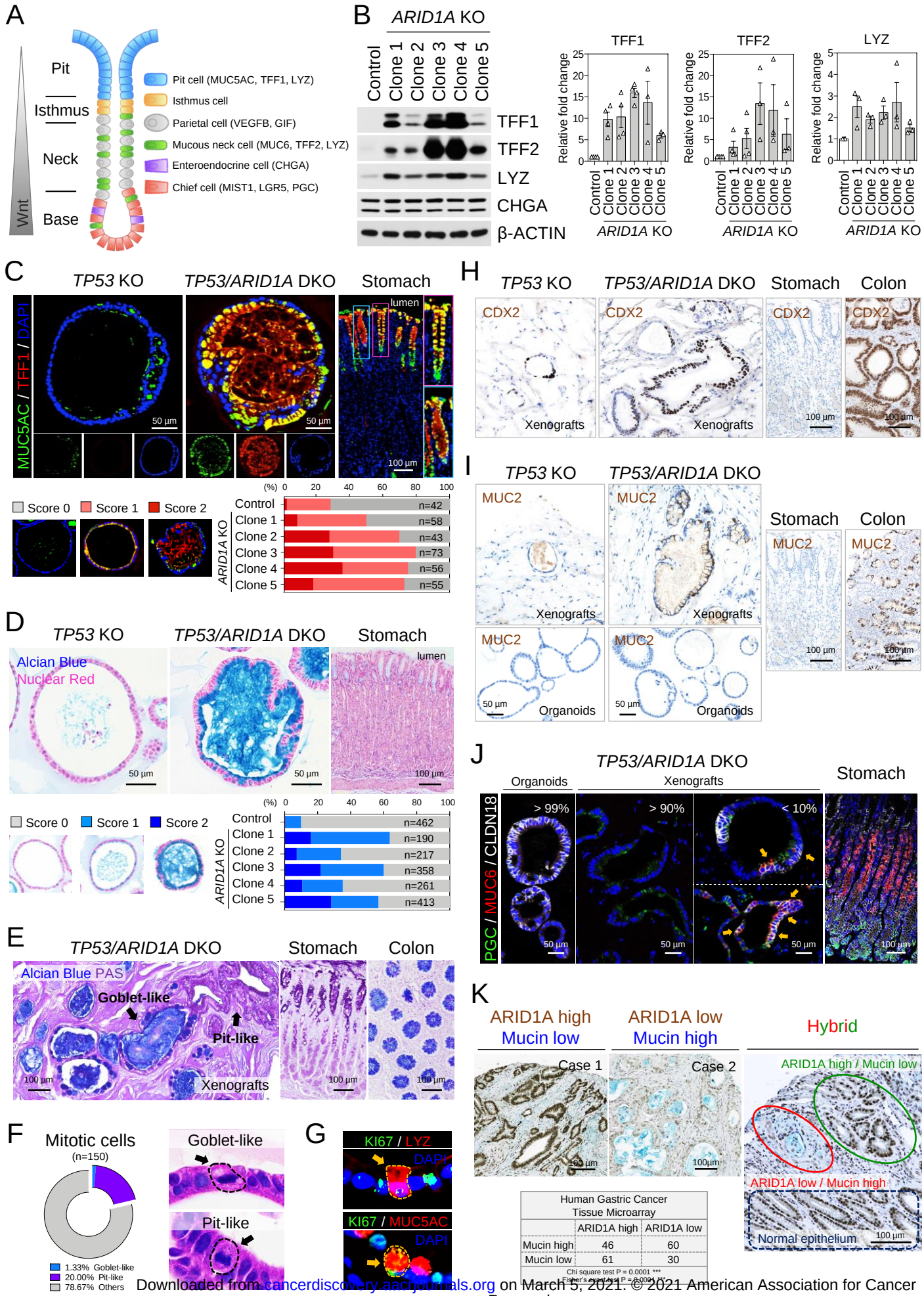

# Figure 4

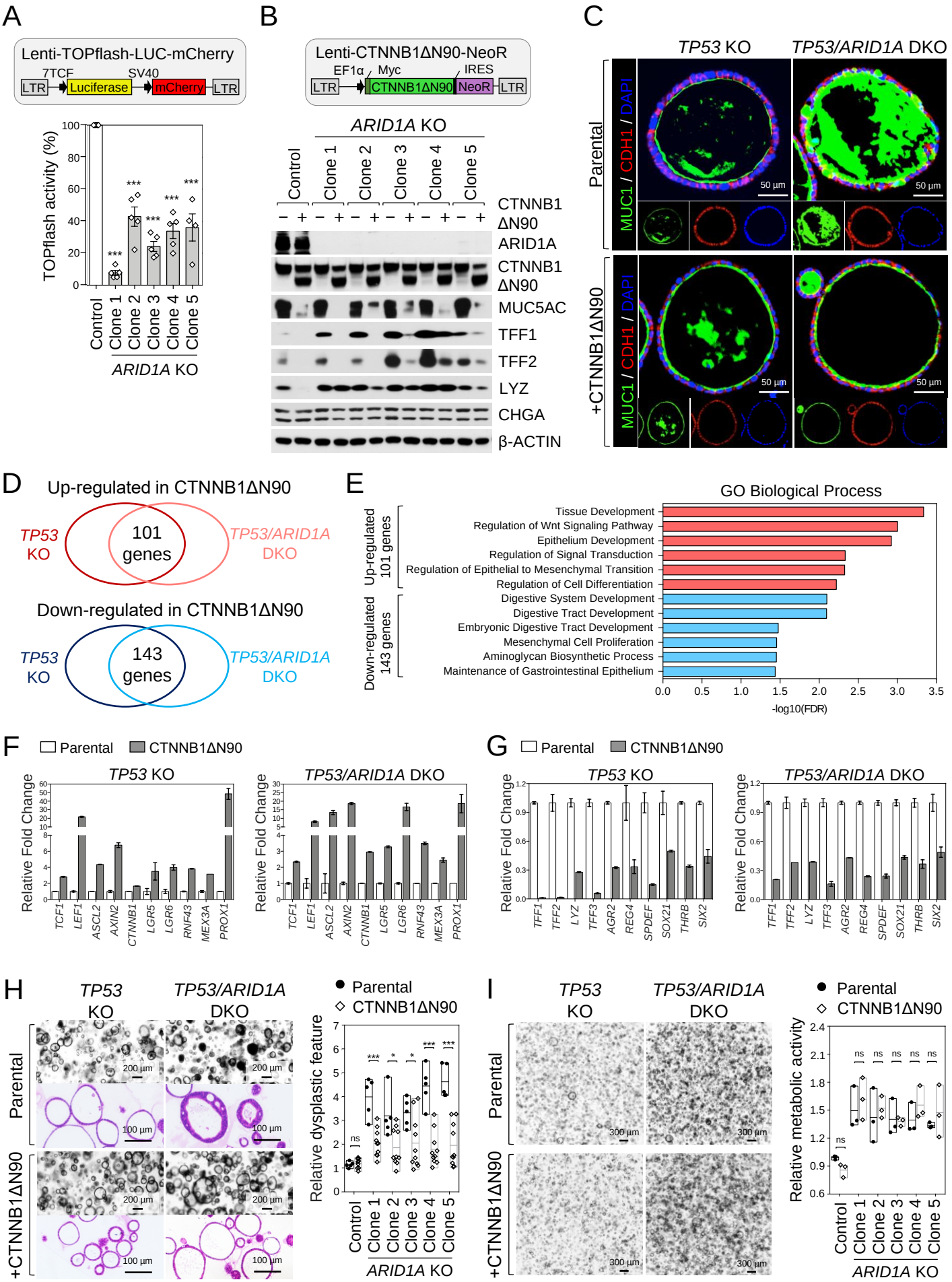

# Figure 5

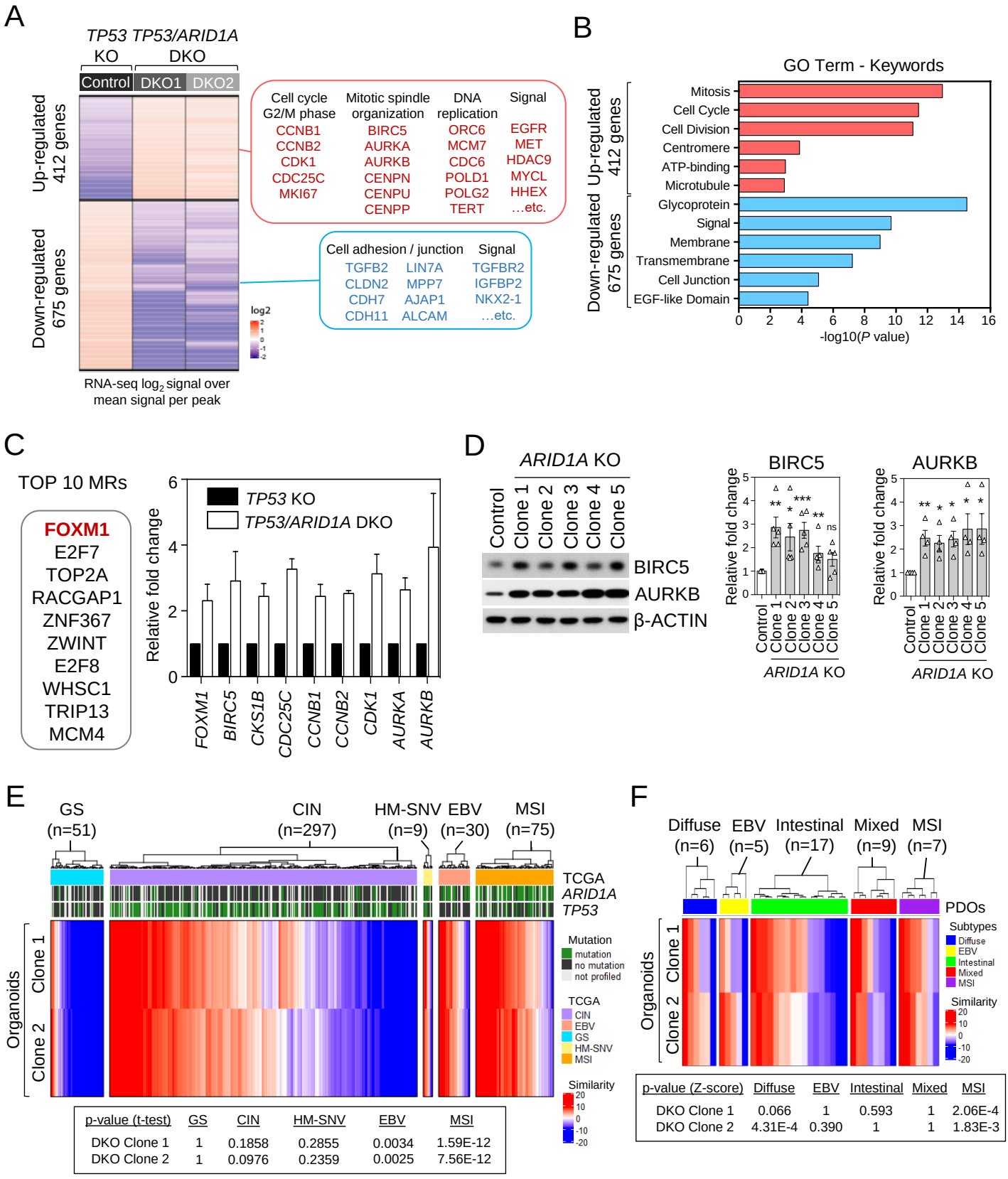


| p-value (t-test) | GS | CIN | HM-SNV | EBV | MSI |
|---|---|---|---|---|---|
| DKO Clone 1 | 1 | 0.1858 | 0.2855 | 0.0034 | 1.59E-12 |
| DKO Clone 2 | 1 | 0.0976 | 0.2359 | 0.0025 | 7.56E-12 |

| p-value (Z-score) | Diffuse | EBV | Intestinal | Mixed | MSI |
|---|---|---|---|---|---|
| DKO Clone 1 | 0.066 | 1 | 0.593 | 1 | 2.06E-4 |
| DKO Clone 2 | 4.31E-4 | 0.390 | 1 | 1 | 1.83E-3 |

# Figure 6

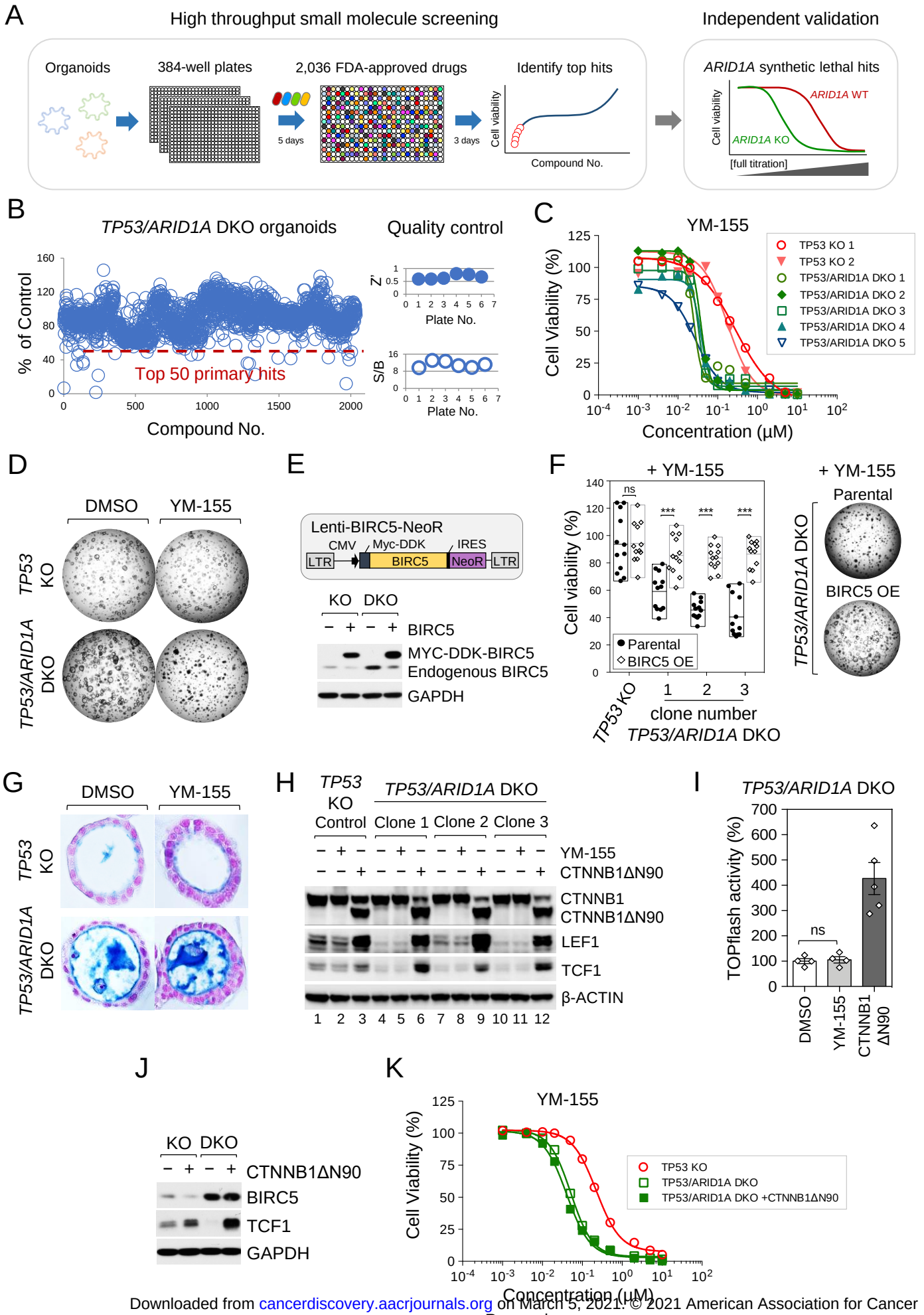

Figure 7

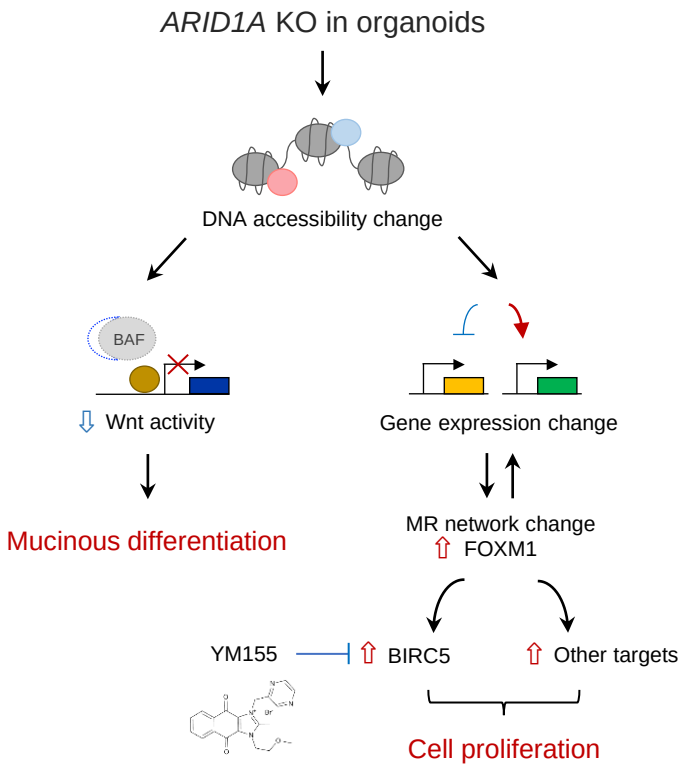

Author Manuscript Published OnlineFirst on January 15, 2021; DOI: 10.1158/2159-8290.CD-20-1109
Author manuscripts have been peer reviewed and accepted for publication but have not yet been edited.

AACR American Association for Cancer Research

CANCER DISCOVERY

# A CRISPR/Cas9-engineered ARID1A-deficient human gastric cancer organoid model reveals essential and non-essential modes of oncogenic transformation

Yuan-Hung Lo, Kevin S. Kolahi, Yuhong Du, et al.

*Cancer Discov* Published OnlineFirst January 15, 2021.